The Shiant Isles Main Sill: structure and mineral fractionation trends

F. G. F. GIBB

Department of Earth Sciences, University of Sheffield, Brookhill, Sheffield S3 7HF, UK

AND

C. M. B. HENDERSON

Department of Earth Sciences, The University, Manchester M13 9PL, UK

Abstract

The Shiant Isles Main Sill, of Tertiary age, is a classic example of a composite, differentiated alkaline basic sill. The first unit to be intruded was a 2 m thick olivine teschenite which was emplaced with phenocrysts of olivine ($mg > 83$) [$mg \equiv$ Mg#] and, perhaps, plagioclase. This was intruded by a 24 m thick picrite sill consisting of a mush of melt and suspended olivine phenocrysts ($mg > 83$) with a D-shaped modal profile. The 140 m thick picrodolerite-crinanite unit was formed by a magma carrying $\sim$ 10% olivine ($mg > 83$) as the main phenocryst phase, together with some calcic plagioclase phenocrysts, being emplaced into the top of the picrite unit before the host rock was completely solidified. The olivine phenocrysts settled towards the bottom to form the picrodolerites. *In-situ* differentiation processes occurred under conditions of almost perfect fractional crystallization, during which very strongly zoned ophitic crystals of olivine (fayalitic rims) and clinopyroxene (hedenbergitic rims), and zoned laths of plagioclase (anorthoclase rims), formed. The last unit consists of $\sim$ 2 m of granular olivine picrodolerite which was intruded into the upper crinanites, again before the host rock was fully solid.

The mineral zoning patterns are interpreted using published cation diffusion coefficient data, and used to show that the picrite unit might have cooled to the blocking temperatures for Mg and Fe diffusion in < 5 years, and that even the relatively thick crinanite unit cooled very fast, so preserving the zoned Fe-Mg olivine and pyroxene compositions. The compositions of coexisting ilmenites and spinels define a redox trend which initially lies close to fayalite-magnetite-quartz buffer conditions, but later becomes more reducing and approaches magnetite-wustite buffer conditions. The final stages of development occurred during sub-solidus deuteric processes and involved formation of analcime and zeolites, as well as localized sulphide mineralization.

KEYWORDS: Differentiated basaltic sill, olivine, clinopyroxene, plagioclase, extreme zoning, multiple intrusion, spinel-ilmenite thermobarometry.

Introduction

THE Shiant Isles, 24 km north of Skye, are formed of four alkaline basic sills of Paleocene/Eocene age intruded into Lower Jurassic sediments (Gibb and Henderson, 1984). These are some of the northernmost members of the Little Minch Sill Complex (Gibb and Gibson, 1989) and one of them, the 'Main Sill', forms most of the islands of Garbh Eilean and Eilean an Tighe (Fig. 1). Walker (1930) recognized that the "Great Sill of Garbh Eilean and Eilean an Tighe" (i.e. the Main Sill) was strongly differentiated and attributed this to gravitative accumulation of olivine. Over the next 50 years, the lower margin (Drever and Johnston, 1959), the basal picrite (Drever and Johnston, 1965), and the mineralogy (Johnston, 1953; Murray, 1954; Gibb, 1973) of the sill were studied. However, relatively little is known about the chemistry of the sill, even though it has often been cited as an example of the differentiation

Mineralogical Magazine, February 1996, Vol. 60, pp. 67–97

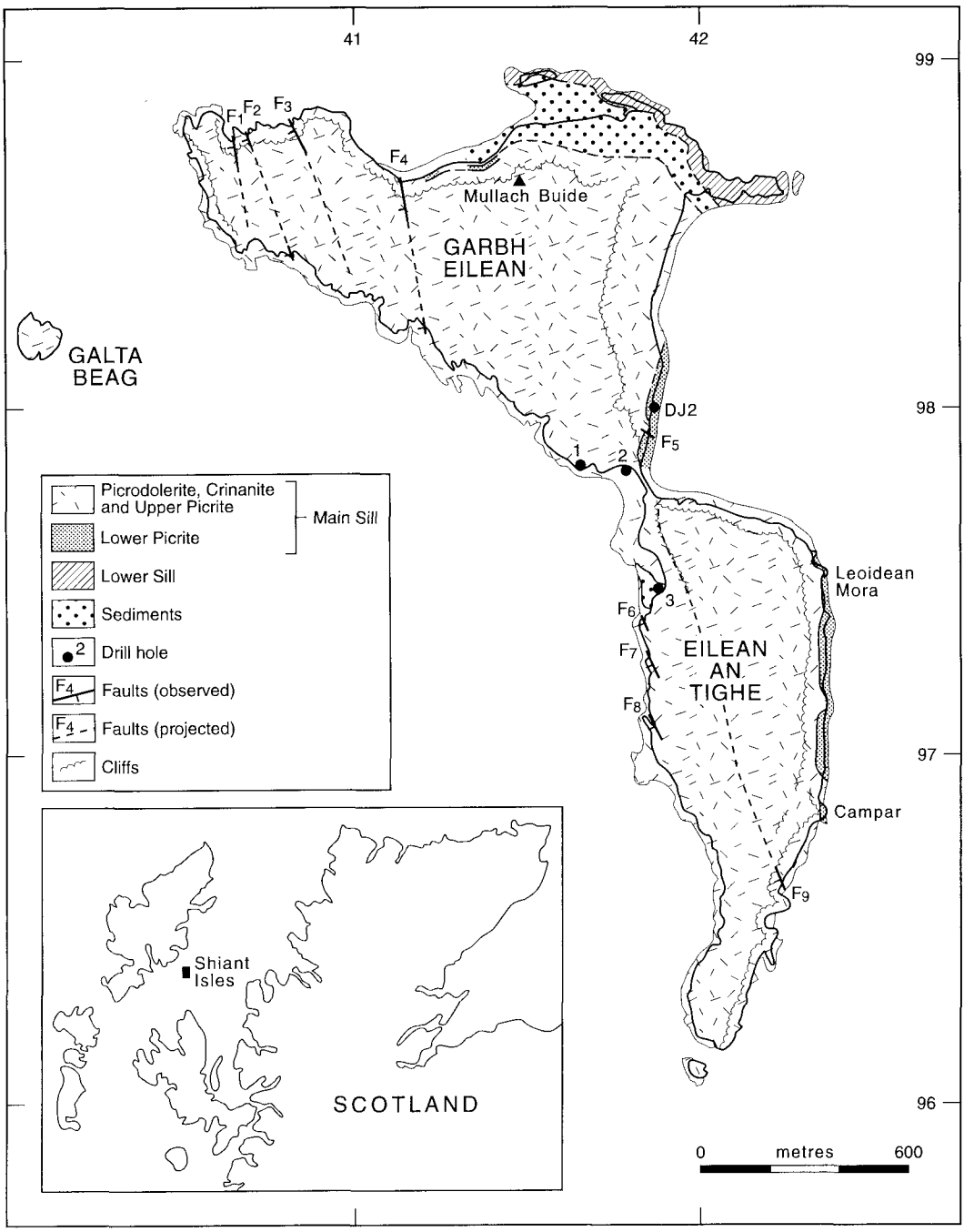

FIG. 1. Geological map of Garbh Eilean and Eilean an Tighe, Shiant Isles, showing the positions of Drill Holes 1, 2, and 3 and of Hole DJ2 (Drever and Johnston, 1965). The 'lower discontinutiy' occurs between the top of the lower picrite (denser shading) and the picrodolerite-crinanite unit.

of undersaturated basic magma (e.g. Wilkinson, 1956, 1979; Wager and Brown, 1967; Deer *et al.*, 1978; Kitchen, 1985; Gibson and Jones, 1991). A comprehensive reinvestigation of this classic intrusion is overdue and, therefore, we are making a detailed study of the Shiant Isles Main Sill, during which we have collected new suites of serial samples and drilled three holes through the sill. We have already discussed the general geological structure of the islands (Gibb and Henderson, 1984) and presented evidence (Gibb and Henderson, 1989) that the Main Sill is a multiple intrusion.

In recent years there has been a major reappraisal of the mechanisms responsible for magmatic differentiation with emphasis switching away from gravity settling of crystals and fractional crystallization to fluid phase processes controlled by convection, diffusion and flow. Most attempts to evaluate theoretical and experimental modelling of such processes have been based on layered intrusions (e.g. Huppert and Sparks, 1980; Sparks *et al.*, 1984; Martin *et al.*, 1987; Sparks *et al.*, 1993; Tegner *et al.*, this volume). However, there is increasing awareness that large sills are much better for this purpose (e.g. Marsh, 1988, 1989) since there is usually less uncertainty about dimensions, original magma composition, number of magma pulses, etc. The Shiant Isles Main Sill provides an excellent example of a large, differentiated, olivine-rich, basic sill against which models of magmatic processes can be tested (e.g. Gibb and Henderson, 1992). In this paper we review the petrographic variation and internal structure of the sill and present a detailed account of the mineral fractionation trends. It will be followed by a companion paper (in prep.) dealing with the geochemistry of the sill and discussing the petrogenesis of this arguably classic differentiated intrusion.

Field relations

Many of the field relations have been described in detail elsewhere (e.g. Walker, 1930; Drever and Johnston, 1959) as has the general structure (Walker, 1930; Gibb and Henderson, 1984). The general dip of the sill on Garbh Eilean is between 5 and 12° to the SSW; the dip swings round northwards so that at the southern end of Eilean an Tighe it is between 10 and 15° NW. On Garbh Eilean the Main Sill (hereafter referred to simply as the sill) is separated from the Lower Sill (Gibb and Henderson, 1984) by between 30 and 40 m of sediment (Fig. 1). On Eilean an Tighe it forms the entire island except for a small outcrop of sediment on top of the sill at the NW corner. The contact between this sediment and the underlying sill represents the roof of the sill (Gibb and Henderson, 1989). By correlating different sections through the sill (see below), we estimate that the thickness is ~ 170 m in the central area of the sill. All thicknesses and heights referred to below are vertical parameters; values corrected for dip will be between 0.5 and 2.5% less.

Using mineralogical and petrographic criteria, the sill can be internally subdivided into four units (see below). Some of the boundaries between these units are sharp but, to date, the only one found to be traceable in the field is the 'lower discontinuity' (Fig. 1). This junction is well exposed at the base of the cliffs along sections of the east coasts of Garbh Eilean and Eilean an Tighe (Fig. 1) where it tends to occur between 5 and 12 m above high water mark (hwm), although occasionally disappearing below beach level. The lower discontinuity is also exposed sporadically in the grassy slopes above the lower contact on the north coast of Garbh Eilean.

The corresponding internal junction near the top of the sill, the 'upper discontinuity' (Gibb and Henderson, 1989) has so far only been identified in the drill core from Hole 3 (locations of drill holes are shown in Fig. 1) where it occurs at a depth of 4.8 m (Fig. 2). It is almost certainly exposed somewhere along the northwest shore of Eilean an Tighe but, since the textural and grain-size differences across this boundary tend to be less marked than across its lower counterpart, it will be extremely difficult to locate.

Veins of leucocratic pegmatitic material, usually 1–20 cm thick, frequently cut through the sill. These are particularly common in the lower picrite where they tend to parallel the sub-vertical joint pattern although often branching and cutting through the host rock in all orientations. On the east coast of Eilean an Tighe, some of these have been observed to cross the lower discontinuity. At a number of localities, especially along the southwest coast of Garbh Eilean in the vicinity of Drill Hole 1, textural and colour 'layering' occurs, reminiscent of the small-scale layering seen in many large basic intrusions. The layers, which are due mainly to modal variation, are usually a few cm thick with rather indistinct margins and may persist for several metres or be more lenticular and localized. Similar modal variations also occur locally in the Hole 1 and Hole 2 sections. In all the cases we have observed from the main sill, the banding appears to occur above the picrodolerite-crinanite transition (Fig. 2) in the lowermost 20 m or so of the crinanite.

Sections through the sill

Complete sections through the sill could not be collected because of the nature of the exposure and the uncertainties over relations between different parts of the islands. Consequently, we rely on a number of partial sections based on drill cores and serial collections from near-vertical outcrops. The

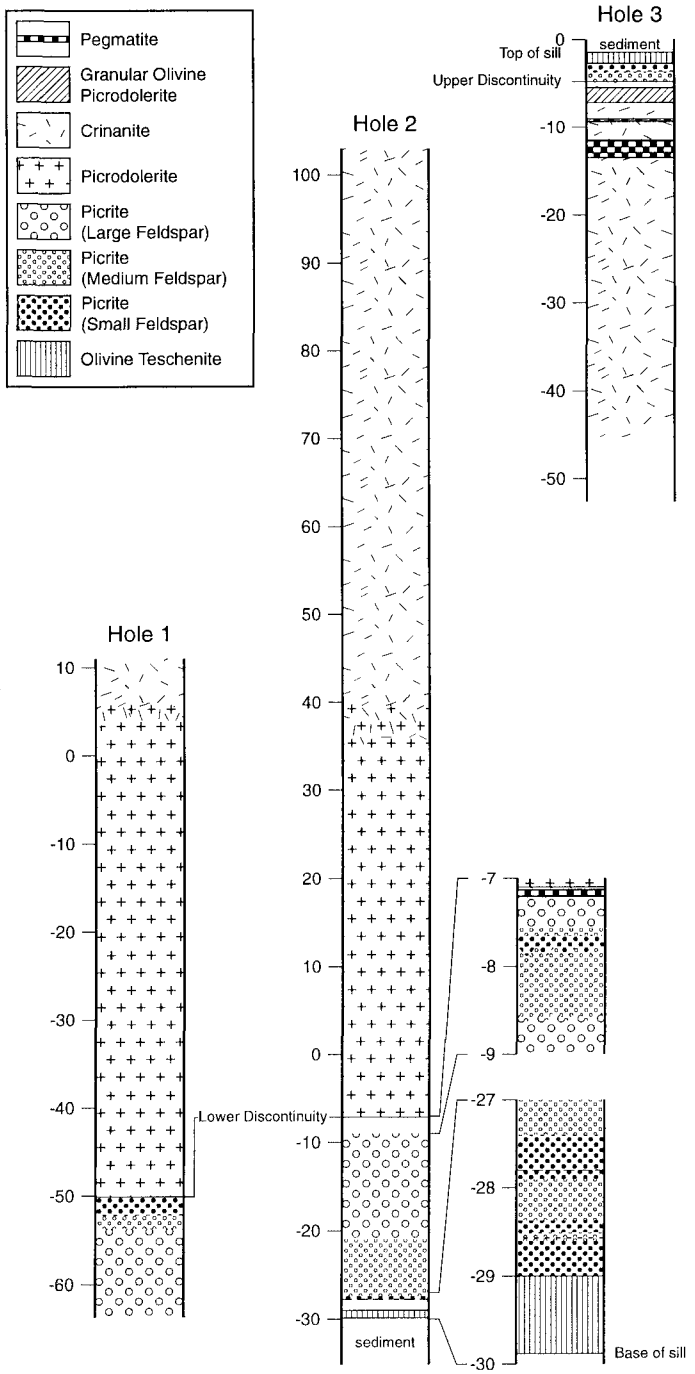

FIG. 2. Simplified vertical sections through the main sill for Holes 1, 2 and 3 and cliff sections above the tops of Holes 1 and 2. Expanded sections from the top and bottom of the lower picrite show the localized alternations of picrite grain size variants. Heights in each section are relative to a zero level at high water mark.

three most extensive of these sections overlap and serve to build up the internal picture of the sill. Their essential features are shown in Fig. 2 and are summarized below. Note that for each of the drill holes the zero level is effectively at the hwm.

Hole 2 section. This section, at the southern end of Garbh Eilean (Fig. 1), consists of drill core from Hole 2 (0 to -30 m) plus a series of specimens collected at intervals from the cliffs immediately above the drill hole (0 to 103 m). From the top of the section to below the 50 m level, the rock is typical Shiant Isles crinanite (Gibb and Henderson, 1984, Appendix) consisting of plagioclase, augite, olivine and Fe-Ti oxides with minor analcime, apatite and brownish zeolite. Lath-shaped plagioclases up to 1.5 mm (but typically < 0.75 mm) long are in an ophitic relationship with augites up to (and occasionally exceeding) 3 cm across. Olivine (<15%) occurs as large (up to 10 mm across), strongly zoned crystals. The olivines are in such an extreme ophitic relationship with abundant plagioclase laths that their outer parts commonly appear to be separate interstitial grains, although in optical continuity with the main part of the crystal. This texture is most pronounced higher up in the crinanite. The Fe-Ti oxides can be up to 2.5 mm across and are invariably skeletal. Analcime is very minor and occurs interstitially to the plagioclase laths. Occasionally clusters of smaller (<4 mm) subhedral olivine crystals are observed which lack the extreme ophitic appearance, although they may be slightly sub-ophitic at the edges.

At the 40 m level in the section, the ophitic olivines characteristic of the crinanite are rare and the crystals tend to be more subhedral with sub-ophitic margins. This marks the beginning of a transition to picrodolerite (Fig. 2). By the 34 m level the olivines are nearly all subhedral to euhedral with only a slight tendency to a marginal sub-ophitic relationship with the plagioclase. Plagioclase laths are typically < 0.5 mm (maximum = 1.2 mm) and from here down to the lower discontinuity (-7.1 m) the rock is picrodolerite with olivine contents in excess of 15%. The increase in olivine content and a slight decrease in the size of the plagioclase continue downwards so that around the 5 m level the rock is typical picrodolerite with ~ 25% olivine in the form of subhedral/euhedral crystals up to 2.5 mm across. Plagioclase occurs as 'stubby' laths (maximum length = 0.9 mm), often in an ophitic texture with large (up to 15 mm) augites (Gibb and Henderson, 1989, Fig. 5*a*).

Many of the crinanite samples and most of the picrodolerites from between the 80 and 5 m levels contain radiating clusters of plagioclase phenocrysts up to 5 mm long. The olivine content continues to increase downwards so that by the 1 m level of this section it exceeds 40% and immediately above the lower discontinuity (-7.1 m, Fig. 2) it reaches 48%. Such high olivine contents are greater than in the picrodolerite immediately above the lower discontinuity elsewhere (Gibb and Henderson, 1989) and, strictly, the rock should be termed picrite. However, the rock is typical picrodolerite in other respects and, to avoid confusion, we refer to it as 'picrodolerite' (the inverted commas signifying excess olivine).

The junction between picrodolerite and underlying picrite (the lower discontinuity) in the Drill Hole 2 section occurs at −7.1 m but is partly obscured by the presence of a 7–9 cm thick late-stage felsic vein containing phenocrysts of augite, kaersutite and Fe-Ti oxide, which has substantially altered the rocks on either side. The rock series below the discontinuity is more variable than at the 'classic' locality (Gibb and Henderson, 1989) with large-feldspar picrite (LFP), which contains very large poikilitic plagioclases (often > 1 cm) (MacKenzie *et al.* 1982, p.80), passing down through medium-feldspar picrite (MFP) to small-feldspar picrite (SFP) (Gibb and Henderson, 1989 Figs. 5*c,d*) at −7.65 m (Fig. 2). Below this, the rock coarsens again via MFP to LFP which persists from −8.7 m to around −21 m before fining again to MFP. Irrespective of the plagioclase grain size, the olivines are present as euhedral/subhedral crystals, mostly 0.3–2 mm across. In this interval (−8.7 to −21 m) the clinopyroxene is present as large poikilitic crystals (8–15 mm) which enclose olivines and which are sub-ophitic with plagioclases. The downwards decrease in feldspar size continues along with a decrease in olivine content and, around the −25 m level, the latter falls below the 40% definition of picrite (Gibb and Henderson, 1984 Appendix). However, as the rock is otherwise typical MFP and is clearly part of the same unit we refer to it as MF′P′. The decrease in plagioclase size then becomes more marked with MF′P′ grading into SF′P′ (small-feldspar, olivine-poor 'picrite') which persists down to −27.8 m. Noticeable throughout the lowest 0.3 m of this SF′P′ are numerous small, slightly coarser patches. At −27.8 m there is a slight increase in plagioclase size and down to −29 m SF′P′s and MF′P′s alternate (Fig. 2).

At −29 m, SF′P′ is succeeded downwards by a very altered, medium-grained rock lacking fresh olivine but with 10–20% of green/brown pseudomorphs after olivine. The pyroxene in this rock occurs mainly as subhedral to ophitic crystals (up to 2.5 mm across); this is a separate unit of olivine teschenite. There are decreases in grain size and amount of olivine pseudomorphs, and an increase in the amount of alteration downwards to the lower contact of the sill where the teschenite is all but unrecognizable. The bottom of the sill occurs at a depth of −29.9 m.

Hole 1 section. This section, 130 m west of Hole 2 (Fig. 1), consists of core from Hole 1 (0 to −63.7 m)

plus specimens collected from an 11 m high, near-vertical face above Hole 1. The rock at the top of the section is crinanite, almost identical to that around the 48 m level in the Hole 2 section. Just below this ophitic olivines become rare and between the 5 and 3 m levels the rock grades into typical picrodolerite. This picrodolerite (complete with stellate clusters of plagioclase phenocrysts) extends down to about the −43 m level by which point the stellate plagioclases have disappeared and the olivine content has risen to 40%. 'Picrodolerite' then continues downwards to at least the −50 m level. The lower discontinuity is much less easy to locate in this section than usual because the underlying picrite is a fine-grained variant of SFP which is difficult to distinguish from 'picrodolerite'. However, we place the discontinuity at −50.1 m based on plagioclase grain-size variation. Below the discontinuity, the plagioclase size increases so that by −52.1 m the rock is more typical SFP; by −52.3 m it is MFP and by −53.7 m it is LFP with large poikilitic feldspars. The LFP persists to the bottom of the drill hole.

Hole 3 section. The top of the sill occurs in Drill Hole 3 at a depth of −1.45 m where the chilled margin consists of a very fine-grained rock containing 14% of olivine as euhedral phenocrysts up to 0.75 mm across. A few mm below this the plagioclase laths in the groundmass have increased from <0.1 mm to between 0.3 and 0.7 mm long, the olivine content has fallen to <4% and the rock has lost its porphyritic appearance; the clinopyroxene forms subhedral to ophitic crystals, with a tendency towards skeletal form, and has paler and darker pink-brown regions. This rock is olivine teschenite with a higher plagioclase:pyroxene ratio than that found around the −29.3 m level in the Hole 2 section. At −2.7 m there is a change to a fine-grained rock consisting of phenocrysts of olivine (20%, <1.2 mm) and plagioclase (<4%, <2.5 mm) in a fine-grained groundmass of acicular plagioclase (0.2−0.7 mm) and altered ophitic augite. It is not unlike a slightly coarser-grained version of the chilled margin. The change at −2.7 m marks the position of the olivine teschenite/picrite boundary at the top of the sill. With downward increases in olivine content and grain size the fine-grained rock passes via SF'P' into MFP (at −4.4 m) so we regard it as simply a fine-grained variant of SF'P'. The MFP persists down to −4.8 m where it changes abruptly to markedly finer-grained rocks; this marks the 'upper discontinuity'.

Immediately below the upper discontinuity is a very thin zone (5−9 mm wide) of fine-grained rock characterised by small euhedral olivines (30−50%) [see Gibb and Henderson, 1989, p.132] followed by fine-grained crinanite. This olivine-rich crinanite, which is characterized by having plagioclase laths which are slightly more acicular than usual (<0.3 mm long), is followed downwards by a general increase in grain size such that coarser types have plagioclase laths typically 0.8−1.5 mm long. Within this general increase, there are occasional reversals and the rock encloses areas of coarser- and finer-grained crinanite giving the impression that the magma broke up and incorporated partly-crystallized parts of itself during emplacement or solidification (Marsh, this volume). The olivine crystals tend to be sub-ophitic, especially at their margins, and the olivine content of the crinanite varies between 12 and 18%.

Between −5.5 and −7.2 m the rock is picrodolerite quite distinct from the overlying crinanite. The plagioclase laths are usually small (typically < 0.6 mm, but in coarser variants up to 2 mm long) and less elongated than in the crinanite, while the clinopyroxene forms subophitic crystals, normally up to 1.5 mm across but up to 3 mm in the coarser grained variants. The rock also contains 34% of olivine as small euhedral/subhedral crystals which impart a granular appearance. We distinguish this rock from the picrodolerites seen elsewhere in the sill by referring to it as 'granular olivine picrodolerite'. Throughout this unit there are local variations in grain size, abundant zeolite-filled amygdales and numerous patches of much coarser pegmatitic facies, often containing zeolites or glass. Occasionally this coarser rock forms veins up to 1 cm thick and thinner veins of vesicular glass have been observed.

Below the granular olivine picrodolerite the sill reverts to fine-grained crinanite similar to that below the upper discontinuity with 16% olivine, mainly as sub-ophitic crystals. With general downward increases in the size of the plagioclase laths, augites, olivines and the tendency of the latter to be sub-ophitic, and a decrease in the olivine content, the crinanite becomes (by −20 m) typical Shiant Isles crinanite. This, which is almost identical to that at the top of the Hole 2 section, persists to the bottom of Hole 3.

Horizons of pegmatite occur at various levels in the crinanite, the two largest of which are shown in Fig. 2. The commonest type of pegmatite consists of broad laths of plagioclase (5−15 mm long) with sub-ophitic to interstitial augites (of similar size) and large skeletal Fe-Ti oxides with minor pyrrhotite. Euhedral crystals of apatite and large sub-ophitic olivines (invariably altered) occur in the pegmatite but are relatively rare. Late-stage aegirine-augite occasionally forms thin rims on large augite crystals while small discrete aegirine grains occur in interstitial patches. Zeolites and analcime, although present, are surprisingly scarce. In many of the pegmatitic horizons (e.g. at −11.5 to −13.5 m), the pegmatites are interspersed with coarse crinanites. Where they have been observed in the field the pegmatite horizons appear to have sharp boundaries

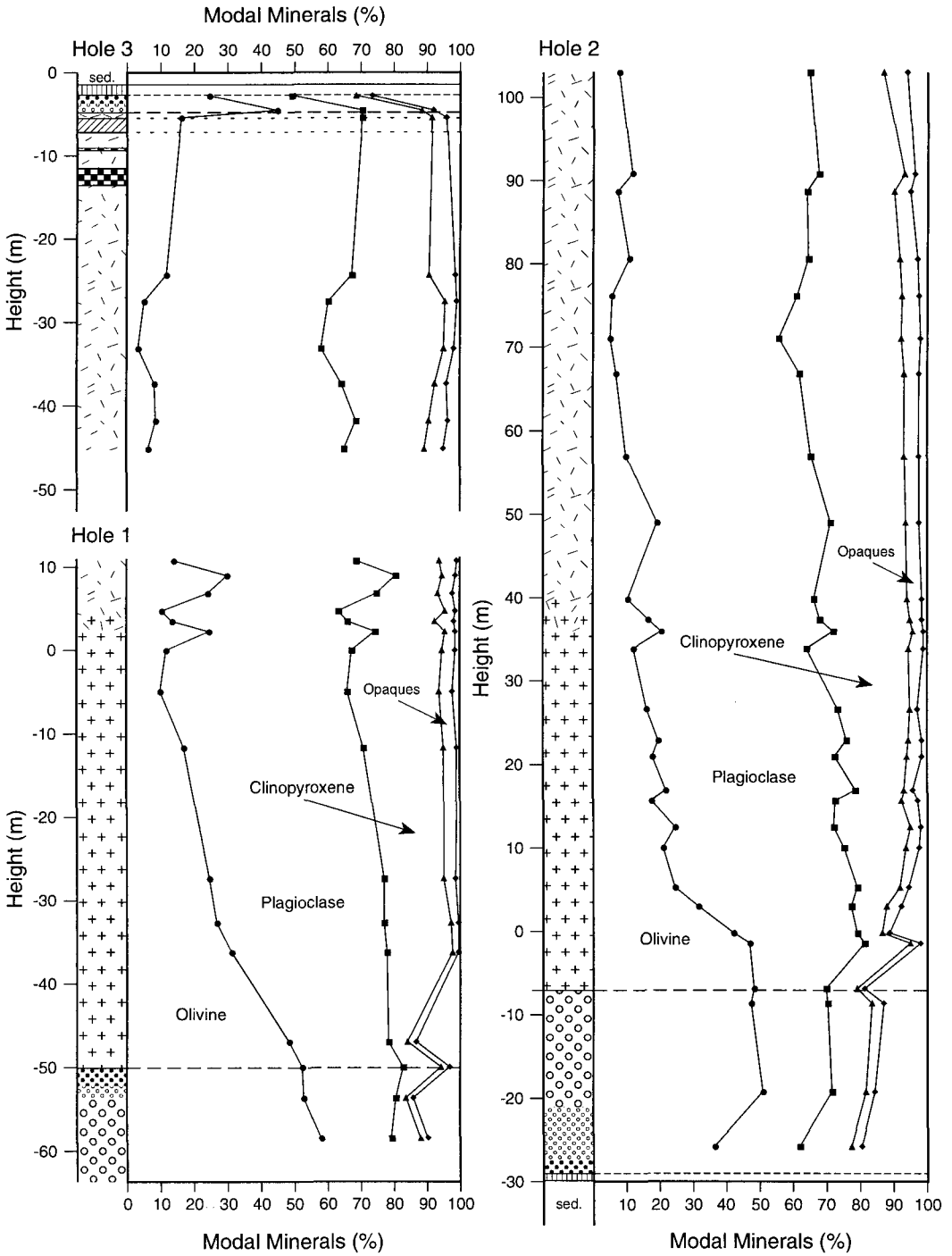

FIG. 3. Modal mineral variations with height for the three sections through the main sill.

with crinanite (or other) host rocks but on the scale of a thin section it can be seen that in some cases the junction is sharp and in others the two rocks merge over a few mm.

Correlation of sections. Apart from the upper and lower contacts, only the lower discontinuity and the picrodolerite-crinanite transition can be correlated readily between the different sections through the sill shown in Fig. 2, but the thickness and sometimes the nature of the various units of the sill vary. At the base of the sill below the picrite, Drever and Johnston (1965) recorded 1.2 m of "fine-grained teschenite" in a drill hole (Hole DJ2, Fig. 1). Teschenite from drill hole DJ2 is considerably less altered, containing fresh olivine, but is texturally the same as the 0.9 m of olivine teschenite at the foot of our Hole 2 section. A sample 0.55 m from the bottom of the sill in Hole DJ2 (sample 47.2) has been used to provide data on the magmatic mineral compositions in the lower olivine teschenite and we will treat these data as though they were from a rock at the bottom of Hole 2.

The thickness of the picrodolerite varies from section to section with the transition to crinanite ranging from $\sim$ 54 m above the lower discontinuity in the Hole 1 section through $\sim$ 44 m in the Hole 2 section to 35 m in the section featured by Gibb (1973, Fig. 1). From -20 m to the bottom of Hole 3 the rock is crinanite, and almost identical to that forming the top 50 m of the Hole 2 section raising the possibility that there is an overlap between the two sections. We have explored this possibility using modal data (below) and whole-rock and mineral chemistry in addition to petrographic criteria and conclude that the best overall fit matches the -40 m level in Hole 3 with the 97 m level of the Hole 2 section. We therefore place the Hole 3 zero at the 137 ± 5 m level of the Hole 2 section (see below).

On the basis of the information reviewed above, we have identified four separate units in the main sill listed in order of intrusion: (1) Upper and Lower Olivine Teschenites (thicknesses 1.2 and 0.9 m, respectively); (2) Upper and Lower Picrites (2.1 and 21.9 m thick, respectively), plus associated pegmatite veins; (3) Picrodolerite-Crinanite, plus associated pegmatites (reconstructed thickness 137 m); (4) Granular Olivine Picrodolerite (1.7 m thick).

Mineralogy

Modal variations

The variations in the amounts of the main minerals with height are shown for the three sections, described above, in Fig. 3. In general the plagioclase:pyroxene ratio appears relatively uniform throughout the sill at 2 ± 0.5, but some systematic variations occur, especially related to the presence of layering near the crinanite-picrodolerite transition, where it fluctuates between about 1.7 and 3.5. The concentration of opaque minerals seems to be fairly constant at around 1% throughout the lower picrite and the lower part of the picrodolerite. It then increases upwards to over 6% in the crinanites around the top of the Hole 2 section and the -25 m level in Hole 3, before decreasing again upwards and into the upper picrite. The opaque minerals are predominantly Fe-Ti oxides but significant amounts of sulphide (mainly pyrrhotite) occur locally, especially in the picrites and picrodolerites near the lower discontinuity, in rocks at the top and bottom of the sill, and in the pegmatites.

Since the variation in olivine content is petrogenetically important (Gibb and Henderson, 1992) we examined it separately using extensive modal analyses. The olivine distributions determined for the Hole 2 and Hole 3 sections have been combined by placing the Hole 3 zero at the 137 m level in the Hole 2 section (see above) to produce a composite profile (Fig. 4). The thickness of the sill in this reconstructed composite section is 165.6 m. In order to facilitate discussion in the context of structural position in the sill, throughout the remainder of this paper all sample heights referred to will be as in the composite section and will be given in italics to distinguish them from actual sampling heights or depths in particular drill holes.

Figure 4 shows that the olivine content increases rapidly upwards from the olivine teschenite at the bottom of the sill into the picrite to a maximum (usually 54–58%) in the LFP before decreasing towards the lower discontinuity. The exact nature of this discontinuity varies from one locality to another (Gibb and Henderson, 1989) but usually the olivine content immediately below it is around 45% while the picrodolerite just above it contains 38–40% olivine. However, in the Hole 2 section, 'picrodolerite' contains 47% olivine and the 'picrite' below has olivine decreasing to $< 40\%$ as the discontinuity is approached.

From the lower discontinuity the olivine content decreases upwards to less than 3% at around the *100 m* level. This decrease is generally steady but there are marked fluctuations (not shown in detail in Fig. 4) around the level of the picrodolerite-crinanite transition due to the small-scale modal layering. Above *100 m* the olivine content of the crinanite tends to increase upwards to 16% just below the upper discontinuity. The olivine content of the granular olivine picrodolerite at about *160 m* appears to be uniform at 34%. Across the upper discontinuity there is a dramatic increase of olivine from 16% in the crinanite to over 50% in the MFP; within the upper picrite, the olivine content decreases upwards to about 20%. In the picrite and olivine

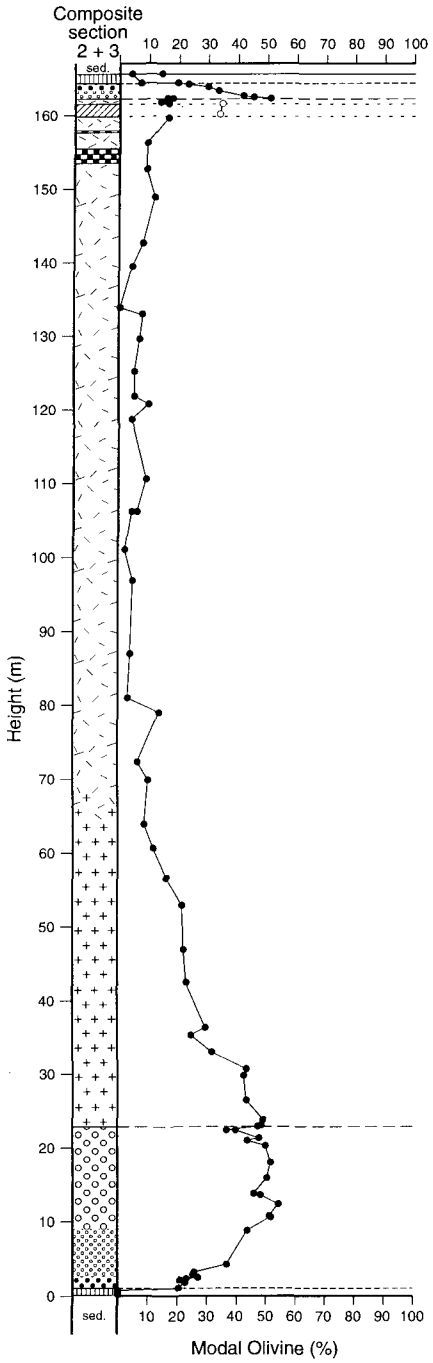

FIG. 4. Modal variation of olivine in the reconstructed composite section through the Shiant Isles main sill. Relative heights are measured from the bottom contact of the sill. Modal data are based on a closer spacing of samples than those shown in Fig. 3.

teschenite above the upper discontinuity the olivine profile is almost a condensed mirror-image of that below the lower discontinuity.

Mineral chemistry

The compositional ranges of minerals have been determined using electron microprobe analysis for 33 samples representing the rock sequence through the sill; most samples are from sections 2 and 3. The majority of the analyses were obtained by energy dispersive methods using either a Cameca Camebax or Cambridge Instruments Geoscan microprobe, both fitted with Link Systems ED detectors. Olivine analyses were mainly obtained by wavelength dispersive (WD) methods with a Cambridge Instruments Microscan 9. Fluorine analyses were obtained by WD using the Cameca. Care was taken to obtain the extremes of composition of the zoned phases but pervasive hydrothermal alteration at the margins of the sill prevented the collection of fully comprehensive data sets, as did deuteric alteration of olivine rims in some samples. It is possible that the most basic centres and/or most evolved rims of very large ophitic pyroxenes might not have been determined and the same may be true for the large poikilitic feldspars in the picrites. Note that the full zoning trends for olivine, pyroxene and plagioclase can be found in a single large ophitic (or poikilitic) crystal, without obvious discontinuities.

Figures 5 and 6 show compositional ranges in olivine, clinopyroxene and plagioclase *vs* height in the sill. Compositional parameters plotted in these diagrams are Mg/(Mg + total Fe) (atom %; denoted *mg* below) for olivine and clinopyroxene (errors approx. $\pm 0.5\%$), and Ca/(Ca+Na+K) (atom %: denoted *An* below) for feldspars (error approx. $\pm 1\%$). In the text, mineral compositional variations are initially dealt with from the bottom to the top of the sill; the relationships between corresponding units from the top and bottom are dealt with further in the next section. Figures 7 and 8 show data for mafic and felsic minerals in representative rocks; in these diagrams not all analyses are plotted to preserve clarity. Individual samples referred to in tables and figures are identified with sample number and height in the composite section.

Olivine. Representative olivine analyses are given in Table 1; note that except for a few samples all data shown are WD analyses so minor element concentrations are reliable down to approx. 0.05%. Figure 5 shows the variation of *mg* and NiO (wt.%) *vs* height in the sill. Olivine from the lower olivine teschenite at *0.55 m* is zoned from *mg* = 80 to 59. In contrast, olivine in the lower picrite is significantly more homogeneous with *mg* restricted to between 83 and 78 except for the sample at the *4 m* level which is

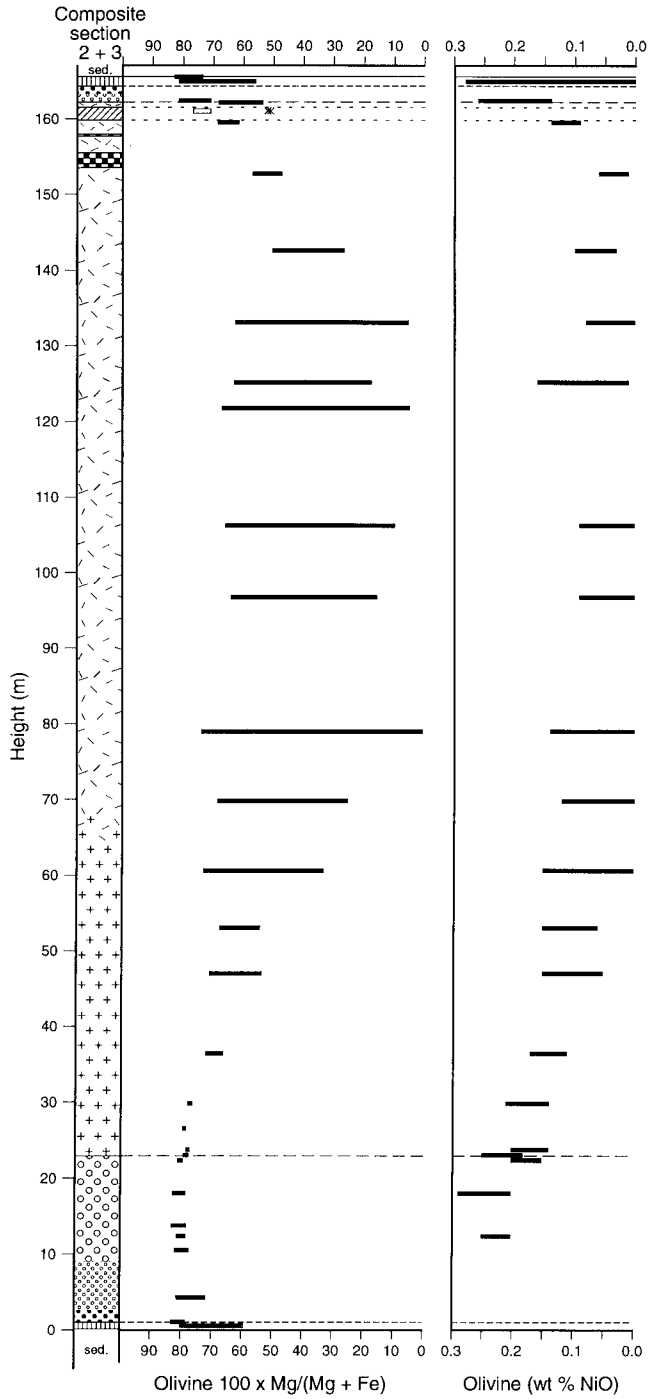

FIG. 5. Variation of Mg × 100/(Mg+Fe) (mole %; denoted *mg* value) and NiO (wt.%) in olivine with height in the composite section through the sill. The ranges of zoning are denoted by the widths of the horizontal bars. The X symbols mark the compositions in the pegmatitic facies of the granular olivine picrodolerite unit.

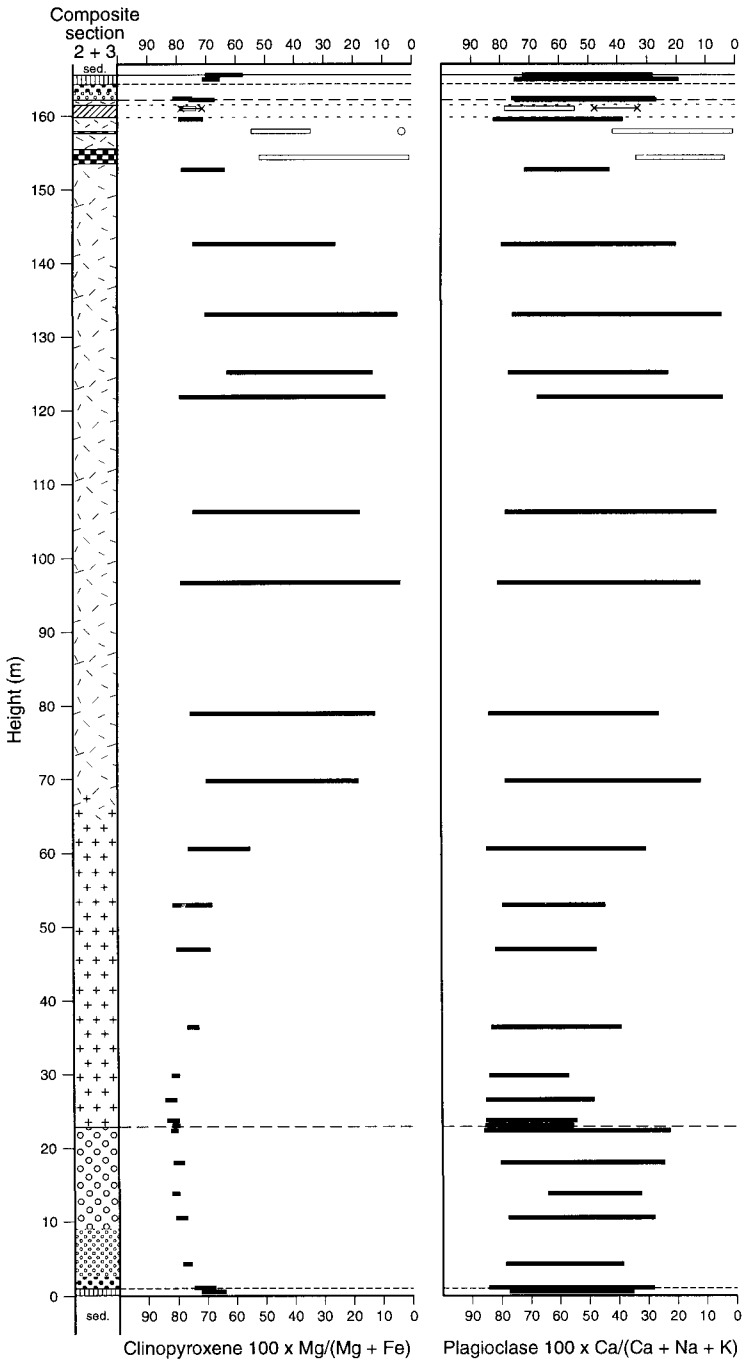

FIG. 6. Variation of *mg* in clinopyroxene and An × 100/(An+Ab+Or) (mole %; denoted *An*) in plagioclase with height in the composite section. Data for the granular olivine picrodolerite and pegmatites are shown with open symbols to prevent confusion with the mineral zoning trends shown by the picrodolerite-crinanite unit. Late stage aegirine-augite and aegirine in the main crinanitic pegmatites plot at the right hand side of the pegmatite data; X symbols as in Fig. 5.

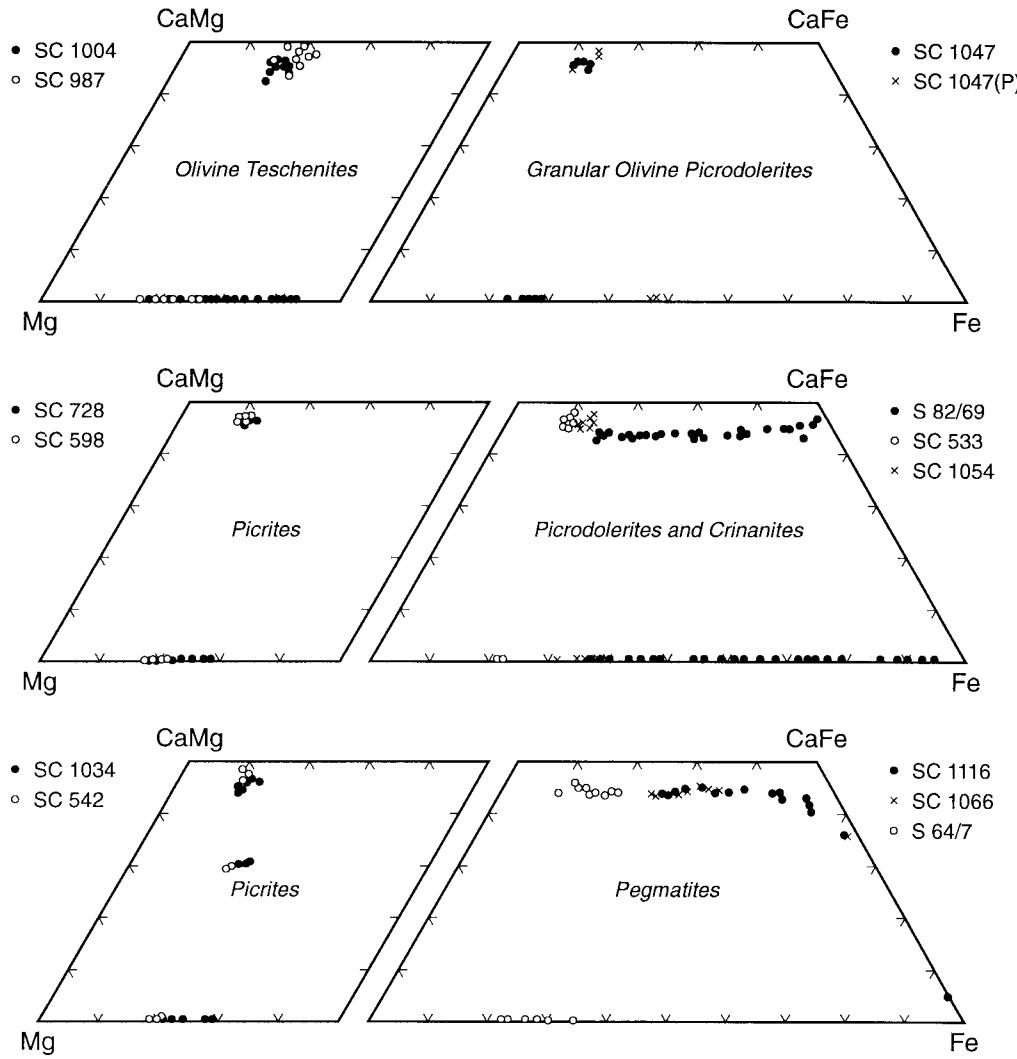

FIG. 7. Ca-Mg-Fe (mole %) compositional variations for mafic minerals in representative samples from each of the intrusive units. Mineral trends for olivine teschenite at the bottom of the sill (Hole DJ2) overlap with those from the upper teschenites and are therefore not shown.

zoned to about *mg* = 71. The larger olivine grains generally have homogeneous *mg* with the lower *mg* values occurring as thin rims. The NiO is significantly more variable than *mg* (Fig. 5; Table 1) showing decreasing contents with lower *mg*, as expected.

Just above the lower discontinuity, the olivines in the picrodolerites show slightly more restricted compositional ranges of *mg* = 79–76; note the most magnesian composition (mg_{max}) compared to that in the picrite. In olivines, from the lowermost picrodolerites, the considerable zoning range for NiO contrasts with the very restricted *mg* values. With increasing height in the picrodolerite and into the crinanite, two striking features are clear. Firstly, mg_{max} averages ~ 71 from the *50* to *80 m* level decreasing upwards to about mg_{max} = 66 at the *95* to *135 m* level. Secondly, the degree of zoning increases upwards so that at *80–135 m* the mg_{min} has decreased to about 5 (Fig. 5). Note that these zoning trends appear to be continuous with the most Fe-rich compositions being represented in the outer parts of

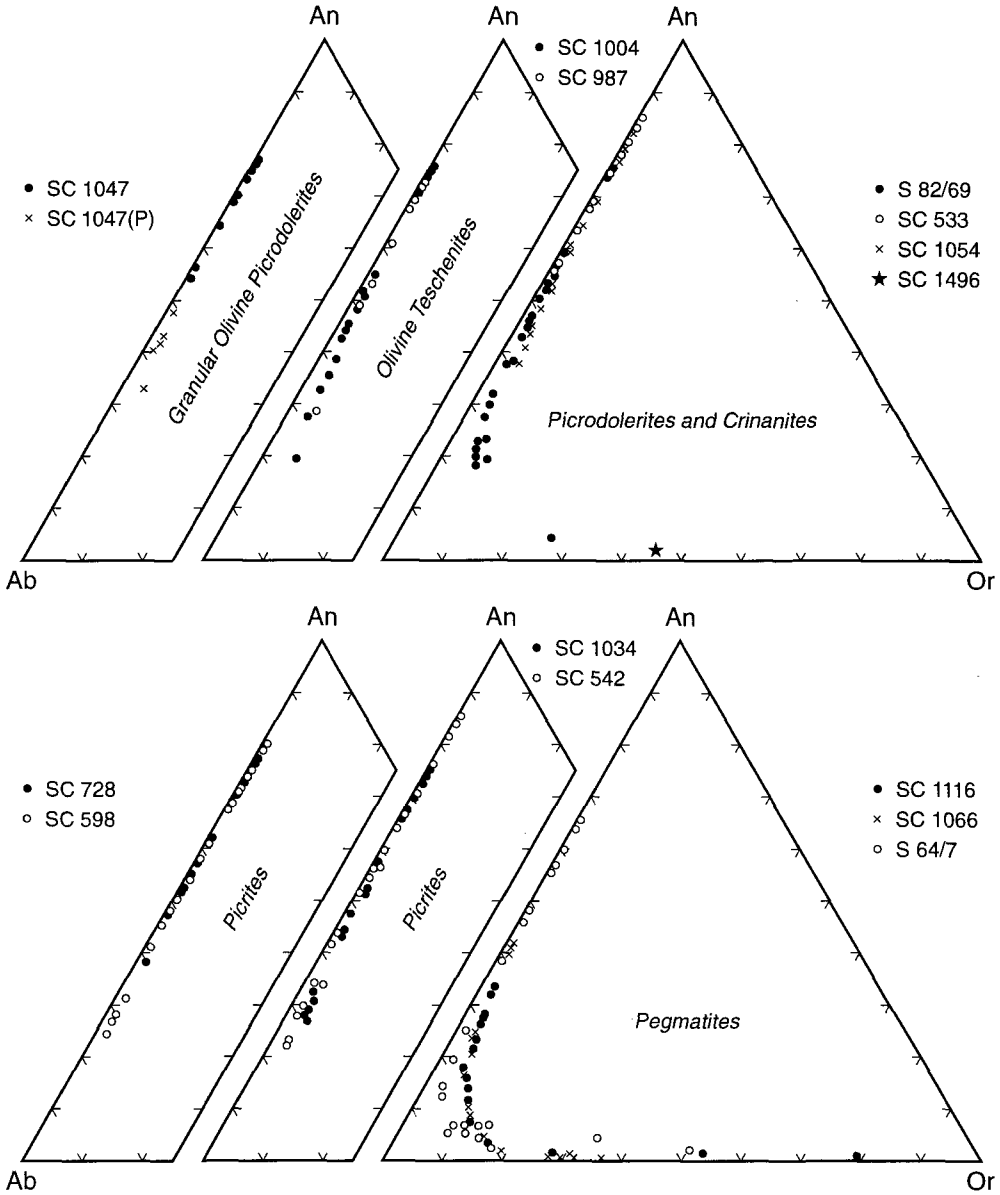

FIG. 8. An-Ab-Or (mole %) compositional variations for feldspars in representative samples from each of the intrusive units. Note that the main feldspar trends are from calcic- to sodic-plagioclase to anorthoclase; potassic alkali feldspars have an extremely restricted occurrence in the crinanitic pegmatites. The star marks the most K-rich alkali feldspar found in the sill in crinanite SC1496; the main feldspar trend in this sample coincides with that for crinanite S82/69.

the extremely ophitic olivines which are characteristic of the crinanites. As *mg* decreases, the Ni content decreases and Ca and Mn increase (Table 1); this is the expected trend in fractionated olivines. Further up the crinanite unit, mg_{max} of the olivine tends to decrease further to 51 at *142 m* before increasing again to 69 at *159 m*. Between *140* and *159 m*, the degree of zoning decreases dramatically. It was not possible to obtain analyses of olivines in the pegmatites at *154.1 m* due to their alteration.

TABLE 1. Representative electron microprobe analyses of olivines

Sample number	LFP SC598		PD SC533	PD S81/25		Crin S82/69		MFP SC1034		OT SC1004		GOPD Peg SC1047		Peg S64/7	
Height in composite section	*17.9 m*		*22.9m*	*46.9m*		*132.9 m*		*162.3 m*		*164.9 m*		*160.9 m*			
SiO_2	39.6	38.9	38.7	38.0	32.9	36.8	30.2	39.2	38.0	39.0	35.8	38.2	35.1	38.8	37.0
FeO	16.2	19.2	19.3	24.3	51.4	32.3	63.8	17.2	25.9	17.2	37.3	23.6	39.5	20.9	30.0
MnO	0.22	0.27	0.3	0.34	0.61	0.46	1.6	0.28	0.4	0.24	0.67	–	0.32	–	–
MgO	43.5	41.1	41.3	37.4	14.4	30.8	3.1	42.8	36.4	42.8	26.6	37.6	23.5	39.7	31.9
NiO	0.28	0.2	0.2	0.12	0.01	0.05	–	0.23	0.15	0.28	0.03	–	–	–	–
CaO	–	–	0.25	0.36	0.48	0.46	1.2	–	–	0.27	0.45	0.34	0.56	0.37	0.27
Total	99.8	99.67	100.05	100.52	99.8	100.87	99.9	99.71	100.85	99.79	100.85	99.74	98.98	99.77	99.17
mg	82.7	79.2	79.2	73.3	33.3	63	5.5	81.6	71.5	81.6	56	74	51.2	77.2	65.5

* Abbreviations for rock names: LFP = Large feldspar picrite; MFP = Medium feldspar picrite; SFP = Small feldspar picrite; PD = Picrodolerite; Crin = Crinanite; OT = Olivine teschenite; GOPD = Granular olivine picrodolerite; Peg = Pegmatite

TABLE 2. Representative analyses of clinopyroxenes

	OT DJ2/472 *0.55 m*		LFP SC589 *17.9 m*		PD SC533 *22.9 m*	PD S81/25 *46.9 m*		Crin S81/34 *96.4 m*		Crin S82/69 *132.9 m*		Peg SC1116 *154.1 m*		MFP SC1034 *162.3 m*		OT SC987 *165.4 m*		GOPD Peg SC1047 *160.9 m*		S64/7	
SiO_2	48.3	48.4	48.7	49.2	50.6	50.6	51.8	47.5	51.5	47.1	50.5	50.4	52.0	49.7	43.4	50.9	49.0	51.3	51.4	51.9
TiO_2	2.1	2.8	2.5	2.6	1.3	1.5	1.0	0.80	1.2	0.69	0.91	1.0	1.2	1.8	4.2	1.2	1.6	1.5	1.1	1.4
Al_2O_3	5.6	5.7	5.0	4.2	3.4	2.0	2.3	1.4	1.7	2.0	1.2	0.78	3.0	5.2	7.8	2.4	4.9	2.4	2.8	2.0
Cr_2O_3	0.13	0.52	0.50	0.66	0.20	–	0.27	–	–	0.10	–	–	0.57	0.55	0.13	–	0.68	0.21	0.59	–
FeO	9.8	6.2	6.3	6.3	8.6	14.3	7.2	26.6	12.5	27.8	19.4	25.8	6.4	6.7	12.6	12.0	6.8	9.0	5.7	10.7
MnO	–	–	0.14	0.03	0.17	0.13	0.20	1.5	0.21	0.41	0.24	–	0.13	0.07	–	–	–	0.15	0.11	0.24
MgO	12.4	14.1	14.4	14.4	14.3	9.9	15.4	1.5	12.0	0.55	7.3	1.7	15.9	14.0	9.7	12.3	14.2	12.8	15.8	12.0
CaO	21.6	21.8	21.7	22.0	21.2	21.5	21.1	20.4	20.8	20.3	21.0	15.5	21.7	22.1	21.3	20.6	21.2	21.8	21.5	20.0
Na_2O	0.68	0.88	1.0	0.92	0.66	0.79	0.71	0.96	0.77	1.2	0.64	4.6	0.47	0.71	1.0	0.93	0.69	0.90	0.66	1.9
Total	100.61	100.40	100.24	100.31	100.43	100.72	99.98	100.66	100.68	100.15	101.19	99.78	101.37	100.83	100.13	100.33	99.07	100.06	99.66	100.14
mg	69.3	80.2	79.9	80.3	74.5	55.0	78.7	9.3	62.8	3.4	39.9	10.4	81.3	78.6	57.9	64.5	78.8	71.4	82.7	66.3

The granular olivine picrodolerite at *161 m* (Table 1; SC1047) has olivine with *mg* in the range 77–71, while the olivines in the associated pegmatitic patches are significantly more evolved (*mg* = 52–51). In the upper picrite at *162 m*, olivine has mg_{max} = 82, similar to that in the lower picrite, as are the Mn and Ni contents (Table 1, cf. data for SC598 and 1034). The degree of zoning is slightly greater than that for samples from the centre of the lower picrite, but exactly matches that for the bottom-most picrites studied (cf. trends at *4* and *162 m*, Fig. 5). Fresh olivine is present in the upper olivine teschenite unit, with the lower sample studied (*165 m*) showing a *mg* range from 82 to 56 compared with 83 to 73 in the upper sample (*165.4 m*).

The Mg:Fe ranges for olivines for representative rocks are also displayed in Fig. 7. Also shown in Fig. 7 (and Table 1) are data for olivine from a sub-vertical pegmatite vein (S64/7) collected from near the top of the lower picrite unit. This pegmatite has olivines which are only slightly more evolved (*mg* = 77–65) than those in the picrite itself (cf. 81–71 at *4* and *162 m*).

Clinopyroxene. Representative compositions for pyroxenes from the different rock types are given in Table 2. Figure 6 shows the variation of *mg* with height in the sill, while Fig. 7 shows the Ca-Mg-Fe trends for selected samples. The Fe:Mg ratios for coexisting olivine and clinopyroxene can be compared in Fig. 7.

The pyroxene in the lower olivine teschenite is slightly zoned from *mg* 73 to 64, with Al_2O_3 and TiO_2 varying in the ranges 2.7–6.6 wt.% and 1.4–2.9 wt.%, respectively, but with no well-defined variation with *mg*; Cr_2O_3 is fairly low at around 0.13 % (Table 2). The pyroxenes in the lower picrite unit generally show more restricted ranges for *mg*, mainly between 82 and 78, except that the pyroxene from the bottom picrite analysed (*1 m*) is less magnesian and more zoned (*mg* = 75–67). Sector-type zoning, visible optically, is reflected compositionally by Ti and Al concentrations varying by up to 15% (relative) with almost constant *mg* (Table 2). The clinopyroxenes in the picrite contain about 0.5% Cr_2O_3 (Table 2). In the pegmatite vein associated with the picrites (S64/7), the cores of large euhedral pyroxenes are as magnesian (e.g. *mg* = 83) as in the picrite itself, with similar Cr contents (Table 2). The rims of these pegmatite pyroxenes are zoned to *mg* = 73 with Na_2O contents of about 1.7 wt.% when adjacent to analcime. Small euhedral crystals included in interstitial analcime are also magnesian (*mg* = 66) and relatively low in Na (Table 2) reflecting the calcic pyroxene differentiation trend (Fig. 7).

In the lowermost picrodolerites (*23–30 m*), the pyroxenes have *mg* values which show little variation (83–79); in this respect, and in their much more variable Cr, Al and Ti contents (up to 30% relative) they are similar to pyroxenes in the picrites below. With increasing height in the picrodolerites, mg_{max} tends to decrease to about 75 at the *60 m* level, while the Cr, Ti and Al contents (Table 2) are smaller than for pyroxenes from lower levels in the picrodolerite (and picrite). Also, the degree of zoning increases upwards so that mg_{min} decreases to a value of 55 at

TABLE 3. Representative analyses of accessory mafic minerals

	Amphiboles				Aenigmatite
	LFP SC674 *10.4 m*	SFP SC542 *22.2 m*	PD SC492 *26.4 m*	MFP SC1034 *162.3 m*	Peg SC1116 *154.1 m*
SiO_2	42.2	42.0	41.7	42.9	38.9
TiO_2	7.0	5.9	5.0	7.0	8.9
Al_2O_3	10.7	11.5	11.4	11.0	1.8
Cr_2O_3	0.27	0.13	–	0.20	–
FeO	9.4	8.2	8.4	8.7	41.9
MnO	–	0.07	–	0.10	–
MgO	13.9	14.9	15.0	13.8	0.68
CaO	11.3	11.2	11.4	11.5	1.2
Na_2O	3.9	4.0	3.9	3.5	6.8
K_2O	0.40	0.41	0.60	0.86	–
F	n.a.	0.37	0.37	0.43	–
Total (less O = F)	99.07	98.52	97.62	99.81	100.18
mg	72.4	76.2	76.1	73.5	2.8

60 m. Within the crinanites mg_{max} in the pyroxenes shows little variation from about 76. However, the trend of increased zoning upwards noted in the picrodolerites is particularly marked in the crinanites extending to *mg* values as low as 5 in the outer parts of the large ophitic pyroxenes at the *95–135 m* levels. As *mg* decreases, Cr, Ti and Al decrease (Cr to below its detection limit of ~ 0.15%). Sodium shows either little change or a very small increase, reflecting that the fact that the trend is towards hedenbergite rather than aegirine (Fig. 7; see Gibb, 1973). In the crinanites above the *135 m* level, mg_{max} is still around 75–79 but the zoning range decreases upwards to about *mg* = 71–79 at *159 m*. However, the pegmatite segregations at *154.1 m* show distinctly more evolved pyroxenes with *mg* varying from 52 at the centre to about 40 at the rim of a large, pale grey-green grain; this rim pyroxene contains only 0.6 wt.% Na_2O (Table 2) consistent with a magmatic trend towards hedenbergite (Fig. 7), as in the crinanites proper. Also present are much smaller pyroxene needles zoned from *mg* 32–17 and Na_2O 0.9–2.2%. Some of the large pyroxenes have distinct, discontinuous thin rims of green aegirine-augite with *mg* = 10 and Na_2O content of ~ 4.6 wt.% (Table 2; Fig. 7). During the latest stages of pegmatite development, small interstitial grains of a more aegirine-rich pyroxene (up to 12.5 wt.% Na_2O; Fig. 7 extreme right of pyroxene trend) crystallize in small amounts, sometimes associated with grains of aenigmatite (Table 3).

The clinopyroxenes from the granular olivine picrodolerite and associated pegmatites both have similar ranges of *mg* values (79–73 and 79–71, respectively), but the former tend to have higher Al_2O_3 and Cr_2O_3 contents (Table 2). The clinopyroxenes in the thin crinanite horizon, occurring between the granular olivine picrodolerite and the upper picrite, have *mg* = 76–67. Within the upper picrite, the clinopyroxene varies from *mg* = 81 to 74, with a similar mg_{max} value, and similar Cr contents to those in the lower picrites, but a slightly more extended *mg* zoning range (cf. trend at *162 m* to those at *4 – 22 m*, Fig. 6), and lower Ti and Al contents (Table 2). The clinopyroxene in the uppermost olivine teschenites at *165.4 m* shows rather wider *mg* variation than that at *164.9 m* (70–57 compared with 71–65, respectively). These skeletal pyroxenes show significant variations in Ti and Al with the deepest coloured regions having the highest contents for these elements (Table 2) as well as Ca (Fig. 7).

Overall, the clinopyroxenes show a similar near-symmetrical *mg vs.* height relationship to that of olivine with relatively homogeneous, Mg-rich pyroxenes in the picrite and with inward increases in the extent of Fe-enrichment in the picrodolerite-crinanite unit.

Amphibole. Late-stage amphibole occurs, usually as interstitial grains, in small amounts in the lower and upper picrites. It has also been found as late-magmatic rims on augite in one of the lowermost picrodolerites (at *26 m*). Representative compositions are given in Table 3 and displayed in Fig. 7. All analyses contain high TiO_2 (5–7 wt.%) (and Al_2O_3) and are kaersutites, the typical magmatic amphibole occurring in alkali basaltic sills (e.g., Henderson and Gibb, 1987). The *mg* values for these amphiboles show only limited variation and are very similar to those of coexisting pyroxenes (Fig. 7); they tend to have high Na:K ratios but the amphibole from the upper picrite has a lower Na:K ratio than those from the lower picrites (cf. analysis for SC1034 to those for SC542 and SC674, Table 3). The F contents are reasonably consistently close to 0.4 wt.% (Table 3), equivalent to an F/OH atomic ratio of 0.10. Note that amphiboles do not appear to occur in the most evolved rock types, i.e. the crinanites and pegmatites.

Feldspars. Plagioclase feldspar is ubiquitous and representative analyses are given in Table 4. Compositional ranges (*An* content) *vs.* height are shown in Fig. 6 and Ca-Na-K relationships displayed in Fig. 8. The most evolved plagioclase grains tend to have rims zoned to about *An* =10, but rims against interstitial felsic/zeolitic patches are sometimes zoned through anorthoclase to more K-rich compositions (Table 4 and Fig. 8). In addition, K-rich alkali feldspars (Table 4, Fig. 8) are very occasionally found in interstitial felsic patches or at the margins between anorthoclase and zeolitic patches.

Plagioclase in the olivine teschenite at *0.55 m* is zoned from *An* = 77 to 35 (Fig. 6). The most striking difference between the compositions of minerals in the picrites is that the mafic phases show little major element variation while the plagioclase shows extreme zoning. Thus the topmost lower picrite analysed (SC542 at *22 m*) is just below the discontinuity and shows an *An* range from 86 to 22 and this compares with a range of 85–28 for the bottom picrite analysed (SC 760 at *1 m*). However, samples between these picrites have slightly smaller maximum *An* and more restricted zoning. These differences may not be real as SC542 and 760 are small feldpsar picrites so that it is easier to obtain the maximum zoning range than for the samples with large poikilitic plagioclases. The pegmatite vein associated with the picrites (S64/7) has slightly more evolved plagioclase with *An* varying from 66 at the centre to 3 at the rim (Fig. 8).

In the picrodolerite-crinanite plagioclases, the highest *An* contents (84–85) tend to occur in the centres of the large stellate crystals. In the lowermost picrodolerites (*23–30 m*), plagioclase centres average about *An* = 84 with zoning to An_{min} values of 55 to 50. With increasing height in the

TABLE 4. Representative analyses of feldspars

	MFP SC598 *17.9 m*		PD SC533 *22.9 m*	Crin SC1496 *121.7 m*	Crin S82/69 *132.9 m*			Peg SC1116 *154.1 m*			Peg SC1066 *157.8 m*	MFP SC1034 *162.3 m*		OT SC1004 *164.9 m*		Peg S64/7
SiO_2	47.8	61.5	46.8	65.5	49.0	63.8	66.3	59.3	66.4	63.9	66.7	48.1	60.6	49.8	60.3	61.0
Al_2O_3	33.4	24.2	33.5	19.4	32.3	22.8	20.2	24.9	19.1	18.5	19.2	33.1	25.8	31.2	23.5	23.8
Fe_2O_3	0.73	0.34	0.67	0.12	0.57	0.31	0.25	0.38	0.83	0.28	0.79	0.39	0.32	0.27	0.78	0.29
CaO	16.0	5.0	17.0	0.42	15.3	3.8	0.95	6.6	0.31	0.13	0.38	15.3	6.4	14.3	5.6	5.2
Na_2O	2.3	8.3	1.9	6.2	2.7	8.7	8.1	7.4	8.0	2.3	7.6	2.7	8.2	3.3	7.9	8.3
K_2O	–	0.30	0.06	7.8	–	1.1	4.5	0.41	4.7	13.3	5.2	0.03	0.64	0.07	0.64	0.29
Total	100.23	99.64	99.93	99.44	99.87	100.51	100.30	98.99	99.34	98.41	99.87	99.62	101.96	98.94	98.72	98.88
Mol. %																
An	79.2	24.6	83.0	2.0	75.6	18.3	4.5	32.2	1.5	0.7	1.8	75.4	29.1	70.4	27.3	25.2
Ab	20.8	73.7	16.6	53.7	24.4	75.4	70.2	65.4	70.8	20.4	67.6	24.4	67.3	29.2	69.0	73.1
Or	–	1.7	0.4	44.3	–	6.3	25.3	2.3	27.7	78.9	30.6	0.2	3.5	0.4	3.7	1.7

picrodolerite/crinanite unit, the An_{max} tends to decrease slightly and the degree of zoning increases markedly so that between *70* and *135 m* the *An* range is from 77 at the centres of plagioclase laths to 11 at the rims (Figs 6, 8). Even lower *An* values (i.e. down to about 4) occur in plagioclase/anorthoclases present in interstitial patches and next to analcime. Further up the crinanite unit, the degree of zoning decreases again and An_{max} tends to increase (to 82 at *159 m*). The pegmatite segregations at the *154.1 m* level in the crinanite unit are more evolved (cf. the mafic phases) with plagioclase *An* contents varying from 34 to 4 (Figs 6, 8). Pegmatite SC1066 at *157.8 m* contains abundant alkali feldspar averaging $An_1Ab_{69}Or_{30}$ in fine-grained syenitic patches (Table 4).

In the granular olivine picrodolerite the plagioclase has a significantly higher range of *An* contents (79–55) than the more evolved associated pegmatite plagioclases (*An* = 48–33) (Table 4; Figs 6, 8). Plagioclase in the upper picrite studied (*162 m*) is rather less calcic than in the lower picrites and is zoned from *An* 76 to 27. The upper olivine teschenites have feldspars varying from *An* 76 to 19 (*164.9 m*) and 73 to 28 (*165.4 m*).

The K contents of plagioclases from the different rock types scarcely vary, down to *An* values of 50, but below that show subtle differences. For example: the upper picrite plagioclases appear to be slightly richer in Or than plagioclases from lower picrites (cf. SC1034 with SC542, SC598 and SC728, Fig. 8); plagioclases from crinanites and olivine teschenites are richer in Or than plagioclases with similar Na contents from the lower picrites; and, plagioclases with *An* < 30 from pegmatitic facies near the top of the sill (Fig. 8, SC1066, 1116, 1047) are distinctly more potassic than those from the pegmatite associated with the lower picrites (S64/7, Fig. 8). Rocks with plagioclases having elevated Or contents tend to be more evolved than those with less K-enrichment in the plagioclase.

Fe-Ti-oxides. Coexisting titaniferous magnetite (spinel) and ilmentite occur in the lower and upper picrites (and the associated pegmatite veins), in the picrodolerites, and in the lowermost, less-evolved crinanites. By contrast, the most-evolved crinanites (and associated pegmatites), the crinanites at the top of the picrodolerite-crinanite unit, and the upper and lower olivine teschenites contain only a highly titaniferous magnetite. In addition, small chrome spinels, with variable Cr and Al contents, occur as inclusions in relatively large, euhedral-subhedral olivines in the picrite and lowermost picrodolerites and, unusually, in one crinanite (S81/34 at *96 m*). Microprobe analyses showed that ilmenites are homogeneous while spinels are generally finely exsolved (< 3 μm scale) but reliable bulk compositions were obtained by averaging analyses made with a 5 μm microprobe spot and/or moving the sample in the beam. However, some rocks had more coarsely exsolved spinels preventing meaningful bulk compositions being obtained. Analyses for discrete oxides in representative rocks are given in Table 5, while Table 6 contains data for spinel inclusions in olivines. Variations of *mg* number for coexisting ilmenite and spinel (excluding spinel inclusions in olivine) *vs.* height are shown in Fig. 9, and for the variations of the compositional parameters 100 × (chromite + spinel)/(chromite + spinel + ulvospinel) (denoted *Cr+Al*) and 100 × magnetite/(magnetite + ulvospinel) (denoted Fe^{3+}) in Fig. 10. Figure 11 shows a plot of *Cr+Al vs.* Fe^{3+} for all the spinel data, including inclusions in olivine. In the discussion below, the data for the spinel inclusions in olivine will be dealt with after the data for the discrete oxide grains.

The olivine teschenite at *0.55 m* contains homogeneous titaniferous spinel with a low *mg* value and low Cr_2O_3 (Table 5); also present are smaller amounts of a coarsely exolved more Cr-rich spinel with individual spot analyses containing up to 11 wt.% Cr_2O_3. Spinels in the overlying picrite unit have distinctly different compositions to the main spinel in the lower olivine teschenite (Figs. 9, 10). The lowest picrite studied (at *1 m*) contains ilmenite grains showing little internal variation but the spinel grains are coarsely exsolved with spot analyses showing up to 13% Cr_2O_3. The main trend in the picrites is of decreasing *mg* values upwards, with the ilmenites being consistently more magnesian than the coexisting spinels (Fig. 9). Figure 10 shows that the spinels in picrites define trends of increasing *Cr+Al* and decreasing Fe^{3+} upwards. The pegmatite associated with the picrite unit (S64/7) also contains coexisting ilmenite and spinel. As expected, both these phases have lower *mg* contents, and the spinel has lower Cr and Al contents, than the equivalent minerals in the host picrites (Table 5), consistent with the pegmatite phases being more evolved.

The Fe-Ti oxide minerals in the bottom-most picrodolerites have much the same compositions as those in the picrites just below (Table 5; Figs 9, 10). With increasing height in the picrodolerite-crinanite unit, the spinels show a decrease in *mg* from approx. 13 at *23 m* to 1.5 in the most evolved crinanites at the *122–133 m* level. Above this height, the spinels in the upper crinanites show *mg* increasing to a value of ~ 10 in the top crinanite studied (at *162 m*). For the rocks in the picrodolerite-crinanite unit with coexisting ilmenite and spinel, the *mg* values follow similar decreasing trends up to the *105 m* level, but note that ilmenite in crinanite at *96 m* has an anomalously high *mg* value. No ilmenites have been found in the crinanites above *110 m*. Most of the picrodolerite-crinanite unit spinels define clear trends

TABLE 5. Analyses of representative Fe-Ti oxides present as discrete grains

	OT DJ/472 *0.55 m*	LFP SC598 *17.9 m*		PD SC533 *22.9 m*	PD SC533 *22.9 m*	Crin S82/69 *132.9m*	Peg SC1116 *154.1 m*	MFP SC1034 *162.3 m*		GOPD SC1047 *160.9 m*		Peg		OT SC1004 *164.9 m*	Peg S64/7	
	S (5)	S (6)	I (6)	S (6)	I (4)	S (6)	S(4)	S (5)	I (8)	S (4)	I (4)	S (2)	I (5)	S (3)	S (7)	I (5)
SiO_2	0.33	–	0.22	–	0.29	0.61	0.7	–	–	0.25	–	0.36	–	–	0.31	0.24
Al_2O_3	2.3	3.3	–	3.2	–	1.1	1.2	6.4	0.07	5.7	0.07	2.2	0.08	3.8	1.4	0.13
TiO_2	23.8	17.5	50.9	16.1	52.0	30.2	29.5	20.3	53.5	22.5	53.8	28.3	53.3	26.8	20.6	50.8
FeO	70.0	58.1	37.9	62.6	40.4	65.6	62.3	50.4	37.7	49.2	36.9	63.4	40.7	59.6	70.2	43.4
MnO	–	–	–	–	–	–	–	0.47	0.51	–	0.49	–	0.58	–	–	–
MgO	1.5	5.7	6.4	4.9	6.1	0.56	0.7	5.9	6.4	5.8	6.6	2.8	4.3	3.5	2.3	3.4
Cr_2O_3	0.18	8.2	0.79	9.0	0.58	0.1	0.58	14.6	0.73	14.0	0.79	0.32	0.11	3	0.15	0.10
Mole %																
$(Fe,Mg)_2TiO_4$	66.6	48.9	–	43.9	–	86.5	88.0	53.4	–	55.5	–	79.3	–	73.8	59.1	–
$(Fe,Mg)Fe_2O_4$	28.3	31.9	–	36.3	–	10.8	9.2	13.2	–	9.8	–	15.6	–	13.8	37.6	–
$(Fe,Mg)Cr_2O_4$	0.2	12.1	–	13.0	–	0.2	–	20.2	–	22.4	–	0.4	–	4.3	0.2	–
$(Fe,Mg)Al_2O_4$	4.9	7.1	–	6.8	–	2.5	2.8	13.1	–	12.3	–	4.7	–	8.1	3.1	–
$(Fe,Mg)TiO_3$	–	–	96.5	–	95.7	–	–	–	97.8	–	98.4	–	98.7	–	–	96.0
R_2O_3	–	–	3.5	–	4.3	–	–	–	2.2	–	1.6	–	1.3	–	–	4.0
mg	3.6	14.9	23.2	12.1	21.1	1.5	1.6	17.1	22.9	16.8	23.9	7.3	15.7	9.4	5.4	12.4

S = spinel; I = ilmenite; Numbers in parentheses denote numbers of analyses averaged.

TABLE 6. Analyses of representative spinels occurring as inclusions in olivines

	LFP SC598 *17.9 m*	LFP SC642 *13.7 m*	PD SC518 *23.6 m*	PD SC492 *26.4 m*	PD S81/13 *36.3 m*			Crin S81/34 *96.4 m*
SiO_2	–	–	0.26	–	0.26	0.18	0.25	0.15
Al_2O_3	12.4	35.4	24.5	19.0	23.5	8.5	4.3	4.5
TiO_2	4.8	1.5	1.3	1.1	0.93	3.8	11.3	11.4
FeO	43.2	30.7	40.5	45.0	43.5	47.7	56.5	56.1
MgO	8.2	11.7	8.3	7.6	6.8	4.4	4.3	4.5
Cr_2O_3	25.1	19.6	21.2	24.1	20.5	29.9	18.6	18.3
mole%								
$(Fe,Mg)_2TiO_4$	19.6	3.4	3.1	2.7	2.3	10.3	31.2	31.6
$(Fe,Mg)Fe_2O_4$	22.1	12.0	22.7	29.1	25.0	28.5	32.4	32.1
$(Fe,Mg)Cr_2O_4$	33.5	22.9	27.2	31.4	26.8	43.0	27.1	26.6
$(Fe,Mg)Al_2O_4$	24.8	61.7	47.0	36.8	45.9	18.2	9.3	9.7
mg	25.3	40.4	26.7	24.5	21.8	14.2	11.9	12.4

for the variations of $(Cr+Al)$ and Fe^{3+} with height, showing significant initial decreases upwards to *100–135 m*, followed by slight increases (Fig. 10). Thus, spinels from the most evolved crinanites between the *105* and *135* m levels tend to have the highest ulvospinel contents (approx. 87 mol.%; equivalent to 30 wt.% TiO_2) and lowest magnetite contents (10 mol.%) (Table 5). The spinels in the main pegmatite segregations at *154.1 m* have *mg*, $(Cr+Al)$ and Fe^{3+} values similar to those for spinel in the most evolved crinanites. Note that the Fe-Ti oxides, particularly the spinels, show as well-defined evolutionary trends with height in the sill as the major rock forming silicates.

The granular olivine picrodolerite and its pegmatite segregations (SC1047 at *161 m*) both contain coexisting ilmenite and spinel. Both Fe-Ti oxides in this picrodolerite are compositionally very similar to those in the upper picrite (SC1034 at *162 m*) (Table 5; Figs 9, 10) while those from the pegmatite segregations are, as expected, considerably more evolved. The upper picrite contains coexisting spinel and ilmenite both of which have relatively high *mg* values which fall on the trends defined by these minerals in the lower picrite unit (Fig. 9). The composition of the spinel is particularly noteworthy in being simultaneously enriched in TiO_2 (21 wt.%) and Cr_2O_3 (15 wt.%) (Table 5). The $(Cr+Al)$ value for spinel from SC1034 is close to that for the picrite just below the lower discontinuity but the Fe^{3+} ratio is significantly lower (i.e. more reduced). The composition of the spinel from the upper olivine teschenite (*165 m*) is more evolved (i.e. lower *mg*) than that in the nearby upper picrite (Table 5; Fig. 9), together with lower $(Cr+Al)$ and Fe^{3+} values (Fig. 10). In this regard, the teschenite Fe-Ti oxide is similar to those of the less evolved upper crinanites.

The spinel phases occurring as inclusions in relatively large, euhedral/subhedral olivines show a wide range of composition, but are generally relatively primitive in so far as their *mg* values, and the Cr and Al contents tend to be higher than those of other spinel grains in the various rock types (Tables 5 and 6). The highest spinel content found is 61.7 mol.% (35.4 wt.% Al_2O_3), while the highest chromite value is 43.0 mol.% (29.9 wt.% Cr_2O_3). Note that only the euhedral-subhedral olivines from the picrites, picrodolerites, and bottom-most crinanites contain these spinel inclusions, and that high-Cr spinels occur in crinanite as well as in picrodolerite and picrite (Table 6). High-Al spinels were only found as inclusions in olivines from picrites and picrodolerites. Except for a few samples, the coupled variation of $(Cr+Al)$ *vs.* Fe^{3+} for the whole suite of spinels is well defined (Fig. 11), indicating that the tendency is for the most primitive types (highest *mg* values) to be the most enriched in Cr and Al, the most depleted in Ti, and the most oxidized, and vice-versa for the most evolved spinels. The former occur as inclusions in relatively large, euhedral-subhedral olivines and the latter tend to occur in evolved crinanites and associated pegmatites.

Analcime and zeolites. Analcime occurs in minor amounts in all rock types, as an interstitial phase, in thin veins cutting the picrites and altering feldspars in pegmatites, and also in sub-spherical 'amygdales' in rocks close to the top of the sill (e.g. SC1054 at

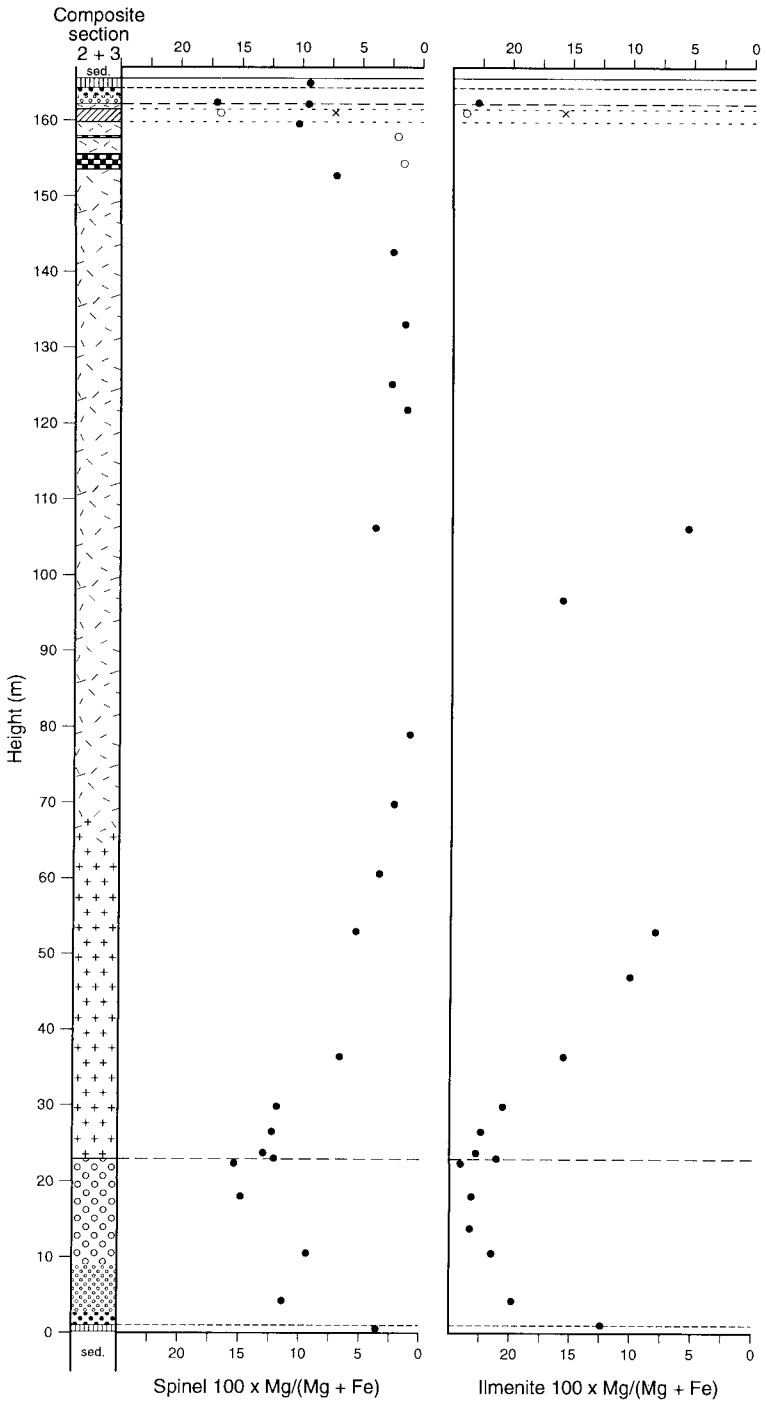

FIG. 9. Variation of *mg* in spinel and ilmenite with height in the sill; open and X symbols as in Figs. 5 and 6.

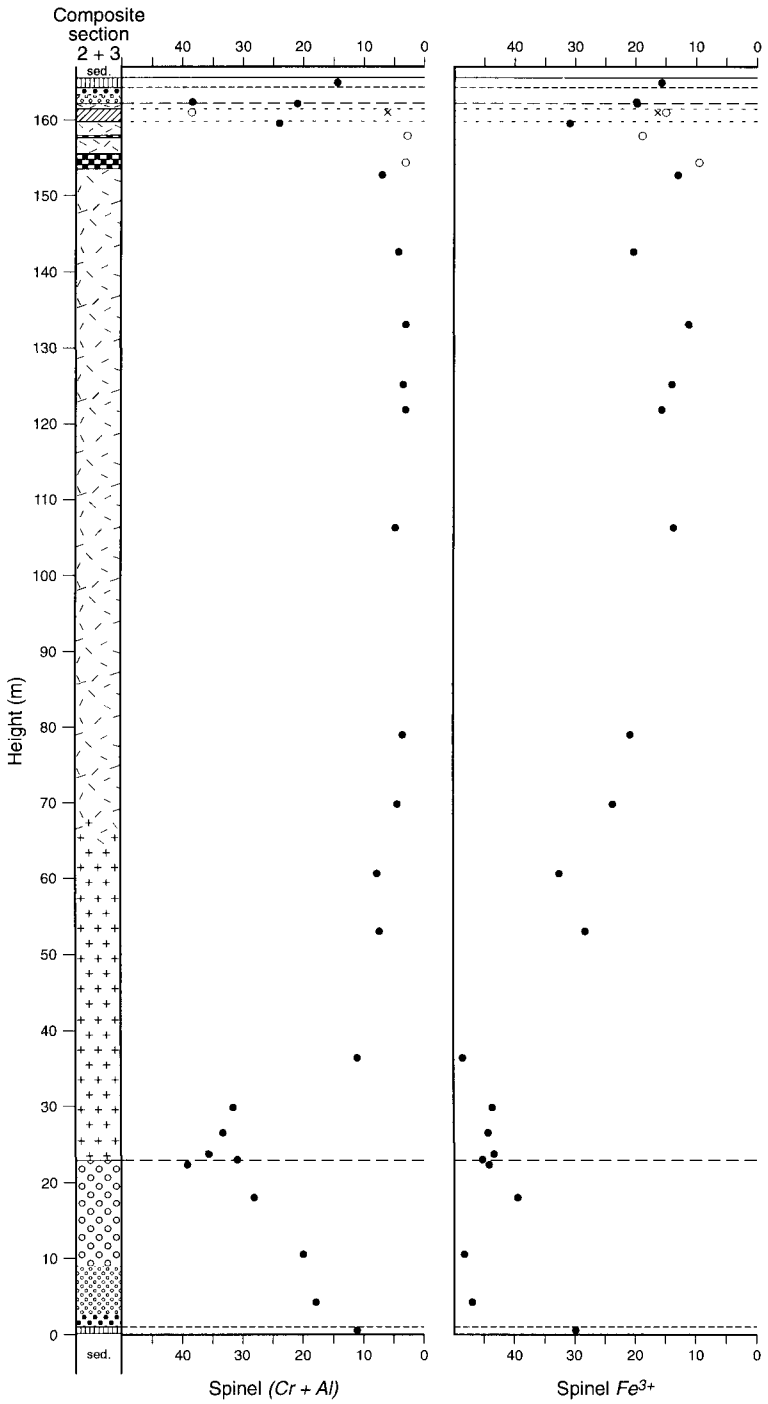

FIG. 10. Variation of 100 × (chromite+spinel)/(chromite+spinel+ulvospinel) (mole %; denoted *(Cr+Al)*) and 100 × magnetite/(magnetite+ulvospinel) (mole %; denoted Fe^{3+}) in spinels occurring as discrete grains with height in the sill.

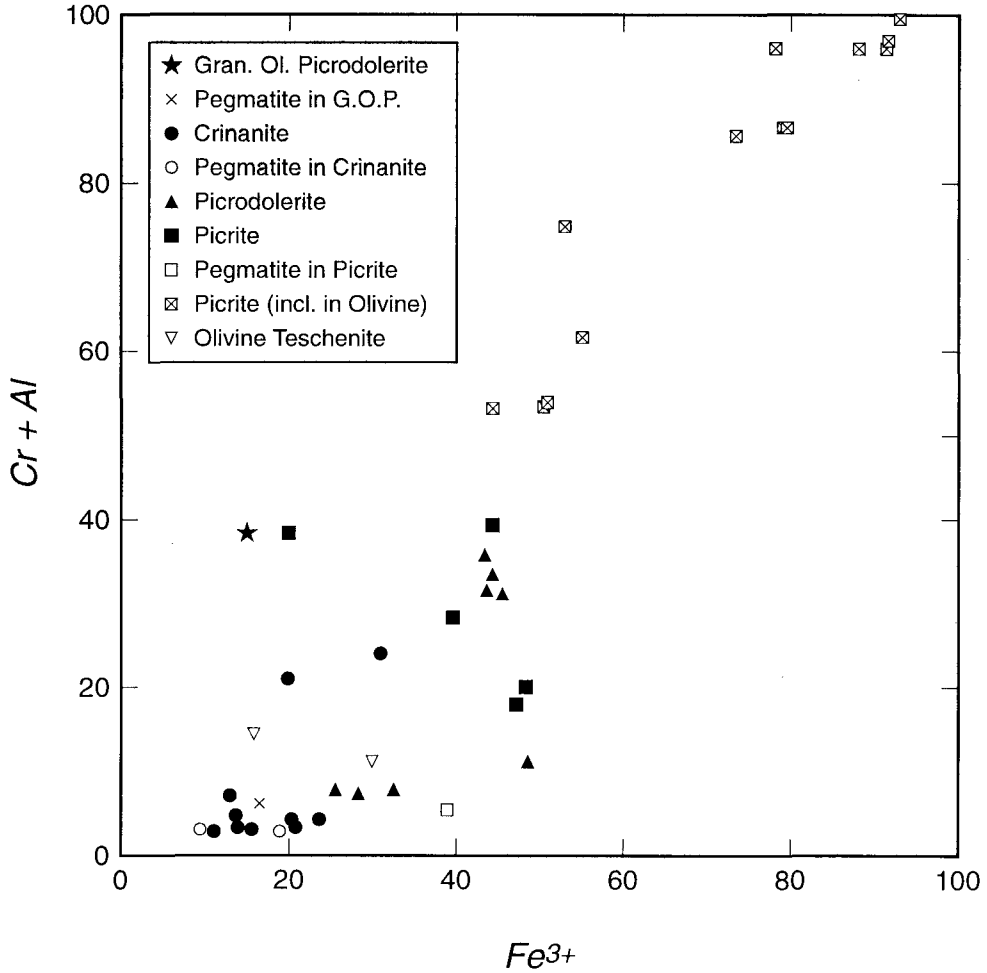

FIG. 11. Variation of *(Cr+Al) vs.* Fe^{3+} for spinels occuring both as discrete grains and as inclusions in olvines. The two points at *(Cr+Al)* ~40 plotting to the left of the main trend are for the upper picrite and granular olivine picrodolerite indicating that these samples formed under more reducing conditions (lower Fe^{3+}) than the main oxide series.

159 m). Typical analyses are given in Table 7 showing small amounts of CaO and Fe_2O_3. In some rocks, particularly the 'amygdaloidal' samples from the top of the sill, Ca-rich zeolites (mainly thomsonite, Table 7) appear to have formed by alteration of the analcime. Interstitial calcic phillipsites (?) occur in small amounts in the picrodolerite-crinanite unit (e.g., S81/25 at *47 m*) but are relatively abundant in a sample of pegmatitic crinanite collected from the northwest shore of Eilean an Tighe near the top of the sill (S81/42, Table 7). All these phases have formed during post-magmatic, deuteric alteration of the primary felsic assemblages.

Accessory minerals

Apatite is present in all rocks types but is most abundant in the most evolved crinanites and pegmatites. It is invariably relatively rich in F ranging from 2.6 wt.% in apatites from picrites to 3.2% in those from crinanites and related pegmatites; these values are equivalent to F/(F+OH) atomic ratios of 0.68–0.88.

Aenigmatite was only found in pegmatite SC1116 (*154 m*) where it appears to be closely associated with aegirine-rich pyroxenes; an analysis is given in Table 3.

Several sulphide minerals are present in the sill, the commonest being pyrrhotite which occurs mainly

TABLE 7. Representative analyses of zeolites

	LFP SC598	Crin S82/69		Crin SC1054		PD S81/25	Crin S81/42		
	Anal.	Anal.	Thom.	Anal.	Thom.	Phill.	Anal.	Phill.	Phill.
SiO_2	52.6	51.8	39.3	52.7	38.1	45.8	55.5	49.0	45.4
Al_2O_3	24.1	25.5	27.5	22.6	26.8	22.5	22.5	20.6	22.4
Fe_2O_3	–	0.21	–	–	0.80	–	0.1	–	–
CaO	1.0	2.2	12.1	0.70	12.1	9.2	0.6	6.5	4.6
Na_2O	12.7	12.3	3.2	12.7	4.0	3.3	12.7	4.8	6.6
K_2O	–	0.35	–	0.15	–	2.6	0.1	3.6	4.0
Total	90.4	92.36	82.1	88.85	81.8	83.4	91.5	84.5	83.0

Anal. = analcime; Thom. = thomsonite; Phill. = phillipsite

near the outer margins of the sill (e.g. in the lower and upper olivine teschenites at *0.5* and *165 m* and lower picrite at *4 m*); it is the only opaque mineral in the topmost olivine teschenite studied (*165.4 m*, only 2 cm from the top contact). Pyrrhotite also occurs in the pegmatite horizons at around *154 m* and in crinanites at *99* and *142 m*. Pyrite was found near the bottom of the picrodolerites (at *26 m*) and chalcopyrite in a crinanite at *153 m* near the main pegmatites; both pyrite and chalcopyrite occur in the lower olivine teschenite studied (*0.55 m*). Chalcopyrite and pentlandite occur in pegmatitic patches in the granular olivine picrodolerite at *161 m* replacing Fe-Ti oxides.

Mineralogical characteristics of the different intrusive units.

Based on field and petrographic relations we have identified four separate intrusive units in the Shiant Isles Main Sill. The upper and lower olivine teschenite units have closely similar olivine, pyroxene and plagioclase compositional relations and are clearly related. The upper and lower picrite mineral compositions are also very similar even though some subtle differences occur. In addition, the mineral compositions of the pegmatite veins cutting the lower picrite show that these too are genetically related. The largest compositional variations occur within the picrodolerite-crinanite unit, together with their associated pegmatites. The mineral compositions in the granular olivine picrodolerite unit, and its associated pegmatitic patches, are distinct from those of the crinanites that it intrudes. In this section we will draw together the mineral compositional relationships for the different intrusive units and make suggestions regarding the different magmatic evolutionary stages they might represent. In the final section we use the mineralogical data to consider the conditions under which the *in situ* differentiation occurred.

Olivine teschenite unit. This approximately 2 m thick unit was the first intruded. Euhedral/ subhedral olivine phenocrysts have relatively primitive cores which are zoned to fairly evolved rim compositions (*mg* = 83–56) and even the chilled margin contains abundant olivine phenocrysts. Clinopyroxenes tend to form skeletal or strongly sub-ophitic crystals and have more evolved compositions (*mg* = 72–57), while plagioclase laths are zoned from fairly primitive cores to very evolved rims (*An* = 76–19). It seems likely that the most primitive olivines and plagioclases were present as phenocrysts in the magma at the time of its emplacement, and that the more evolved rims formed *in situ* by fractional crystallization, during rapid cooling of this first, thin magma pulse. The skeletal and strongly sub-ophitic pyroxene crystallized rapidly after emplacement of the magma so explaining its relatively evolved mg_{max} values. The main opaque mineral in this rock-type is a titaniferous spinel, but this phase is less magnesian in the lower than in the upper teschenite (cf. values for *mg* of 3.6 and 9.4, respectively). The low Cr spinels are likely to have crystallized *in situ* but grains of Cr-rich spinel in the bottom olivine teschenite were most likely emplaced along with the olivine phenocrysts. The most abundant opaque mineral in the altered upper olivine teschenites is pyrrhotite, with no Fe-Ti-oxide occurring close to the upper chilled margin. Pyrrhotite is less abundant in the least altered lower olivine teschenite, but this rock also contains small amounts of pyrite and chalcopyrite. The sulphides are believed to have formed *in situ*, perhaps resulting from the introduction of sulphur from the sedimentary country rocks.

Picrite unit. This was intruded next and split the olivine teschenite unit into upper and lower leaves. The picrite forms a 24 m thick unit and the upper and

lower picrites remained in contact only during the early stages of its *in situ* development. Perhaps the most striking feature of this unit is the near-symmetrical 'D-shaped' modal olivine distribution (Fig. 4). This pattern is, of course, enhanced by reconstructing the original picrite sill from its two separated leaves. Gibb and Henderson (1992) showed that such D-shaped olivine profiles are not uncommon in thin alkaline olivine dolerite sills and suggested that they resulted from the emplacement processes of a crystal mush, without significant modification by post-intrusion crystal settling or mixing via convection. The euhedral/subhedral olivines are invariably primitive (mg_{max} = 83) showing only limited marginal zoning; some of the larger crystals contain inclusions of Cr and/or Al-rich spinels with a range of *mg* values (12–40). These spinel inclusions were clearly present in the olivines prior to intrusion. Clinopyroxenes generally show similarly homogeneous and primitive compositions (*mg* = 82–78) to those of olivine, while plagioclases range from primitive to evolved (*An* = 86–22). The most primitive plagioclase and pyroxene compositions might have been introduced as small phenocrysts present in the intruding magma but their poikilitic textures surrounding olivines indicates that the bulk of these phases crystallized *in-situ*. Although the pyroxene shows little major-element zoning, implying equilibration, the plagioclases, which must have co-precipitated with the pyroxene, are strongly zoned with the most evolved plagioclase compositions occuring at the margins of large poikilitic crystals in the LFP. Discrete grains of primary spinel and ilmenite are present throughout the picrite unit and the most primitive spinels have compositions similar to those included in olivines. Thus the most magnesian (perhaps with *mg* > 12) and the most Cr- and Al-rich spinels might have been emplaced in the crystal mush, while the less magnesian (*mg* < 12) and more Ti-rich species are most likely to represent the compositions which crystallized *in-situ* alongside the ilmenites. Kaersutitic amphibole formed interstitially as a late-magmatic mineral; the late stage melts responsible for its formation must have been more K-rich at the top of the picrites than lower down to explain the lower Na:K ratio of amphibole in the upper picrite. This is supported by the evolved plagioclases having Or contents about 50% greater than plagioclases with similar *An* values from the lower picrites. The pegmatite veins cutting the picrite have mafic mineral compositions closely related to those in the picrite itself but with slightly more evolved mg_{max} values as would be expected if they formed from late-stage melts from the picrite unit. The plagioclase compositions in these pegmatites overlap with the picrite trend and extend it to the anorthoclase range of compositions.

Picrodolerite-crinanite unit. This approximately 140 m thick unit was intruded into the top part of the picrite unit and separated the upper from the lower picrites. As mentioned earlier, the picrodolerites are characterized by the presence of euhedral/subhedral olivine phenocrysts (mg_{max} = 79), while the crinanites contain large, extremely ophitic olivines together with less-common clusters of subhedral olivines, and the lower crinanites may have subhedral cores of olivine with ophitic rims. The *mg* values for olivines show a symmetrical variation with height in this unit. There is an inwards decrease in *mg* coupled with an inwards increase in the degree of zoning. The most evolved olivines occur between the *80* and *145* *m* levels, i.e. in the third quarter up from the bottom of the sill.

Fairly primitive inclusions of spinels with high *mg* values (12–25), and high Cr and Al contents, occur in olivines throughout the picrodolerites but are restricted to the bottom-most crinanites. As described for the picrites, these euhedral/subhedral olivines and their spinel inclusions are likely to have been intruded in suspension in the emplacing magma. Following intrusion, except at the very top of the crinanite unit, these suspended grains were apparently able to settle fast enough to keep ahead of the downward moving upper capture front (Marsh, 1988, this volume); it seems likely that the bulk of the olivine phenocrysts, originally in the upper part of the crinanite-picrodolerite unit settled out. The remaining olivine melt components crystallized *in-situ*, to give the characteristic ophitic olivine textures, under conditions of essentially perfect fractional crystallization, forming the exceptionally wide zoning range (*mg* = 74–5).

The large stellate plagioclases in the picrodolerite-crinanite unit often occur in aggregates with subhedral olivines. The plagioclases have very calcic cores (*An* 85) and were most likely introduced as phenocrysts in the intruding magma, along with the subhedral olivine, while the remaining plagioclase crystallized *in-situ* alongside the ophitic pyroxene. In contrast to the associated clinopyroxenes, plagioclases in the picrodolerites are somewhat zoned (cf. the picrites), with the degree increasing upwards. Within the crinanite part of this unit, *in-situ* almost perfect, fractional crystallization caused the formation of ophitic pyroxenes zoned (towards hedenbergite rather than aegirine) from *mg* = 76 to 5, and plagioclase laths zoned from *An* = 77 to 4. The crinanites with the exceptionally wide zoning ranges in olivine, pyroxene, and plagioclase occur over a very substantial thickness interval from 15% to 65% of the way down the picrodolerite-crinanite unit. The near-symmetrical compositional trends for the minerals, including the Fe-Ti oxides, *vs.* height within the picrodolerite-crinanite (above) results

from the inward *in situ* crystallization of this unit. The pegmatites intruded into the uppermost crinanites have mineral composition ranges more evolved than the adjacent crinanites but very similar to those of the most evolved crinanites occurring 10-20 m lower. These pegmatites are undoubtedly late differentiates from the picrodolerite-crinanite magma, and their origin will be considered below, bearing this in mind.

Granular olivine picrodolerite. This ~2 m thick unit was intruded very close to the top of the picrodolerite-crinanite unit. The olivines are magnesian but somewhat less primitive (mg_{max} = 77) than those found in the picrite and at the bottom of the normal picrodolerite; they are finer grained and no spinel inclusions were found. Pyroxenes and plagioclases are also fairly primitive with mg_{max} = 79 and An_{max} = 79. Coexisting spinel and ilmenite are similar to, but slightly less primitive than, those in the upper picrite. The same mineral assemblage is present in the associated pegmatitic patches but, except for the pyroxenes, the minerals are substantially more evolved.

Although four distinct intrusive units are described, they have clear mineralogical similarities and presumably formed from genetically related parental magmas. They were probably all emplaced containing suspended phenocrysts of olivine (plus associated spinels) of similar compositions suggesting that they were fed from the same magma chamber. It seems likely that intrusions of magmas to form the olivine teschenite, picrite, and picrodolerite-crinanite units were separated by only very small time intervals, before significant degrees of cooling of the host unit could occur. Under these circumstances the later magmas were almost certainly emplaced into the relatively low-yield-strength semi-solid hosts, still well above their solidus temperatures. Some mixing processes may have taken place, on a local scale, between the host and intruding units. The successive magmas must have had similar melt-phase compositions, as there are no marked discontinuities in mineral compositions except that the olivine in the upper picrite is significantly more primitive than that in the crinanite just below.

Conditions of in-situ crystallization and re-equilibration of mineral assemblages

Only limited possibilities are available for geothermometric and geobarometric deductions based on mineral compositions. The most useful data come from the coexisting ilmenite and spinel phases that occur in all the intrusive units except the olivine teschenite. Analyses of these mineral pairs allows temperatures and oxygen fugacities to be calculated (Buddington and Lindsley, 1964, as modified by Powell and Powell, 1977). Oxygen fugacities show a decreasing trend from 10^{-13} atm at 875°C to 10^{-23} atm at 640°C (Fig. 12). All the picrites (and the associated pegmatite S64/7) plot at the high-temperature end, while the picrodolerites span the whole range. This trend represents the sub-solidus re-equilibration of the Fe-Ti oxides, with some of the rocks continuing to react, most likely via a deuteric fluid, to temperatures well below the solidus. Apart from the upper picrite and the granular olivine picrodolerite and its associated pegmatite, the higher temperature assemblages plot very close to, but slightly below, the fayalite-magnetite-quartz (FMQ) buffer (cf. other alkaline olivine basalt sills, e.g. Gamble, 1984; Henderson and Gibb, 1987), while the trend at lower temperatures approaches the magnetite-wustite buffer curve (Fig. 12). We will consider possible explanations for these relations later.

Helz (1982) showed that hornblendes equilibrated with ilmenite ± spinel close to the FMQ-buffer have increasing Ti contents as temperature increases and we have used her calibration to estimate temperatures of ~ 1050°C for the late-magmatic kaersutites occurring in the picrites which we take as an approximation of near-solidus conditions.

Within the picrites, distinctly different zoning characteristics occur in olivine, pyroxene, and plagioclase. Whereas olivine and pyroxene have

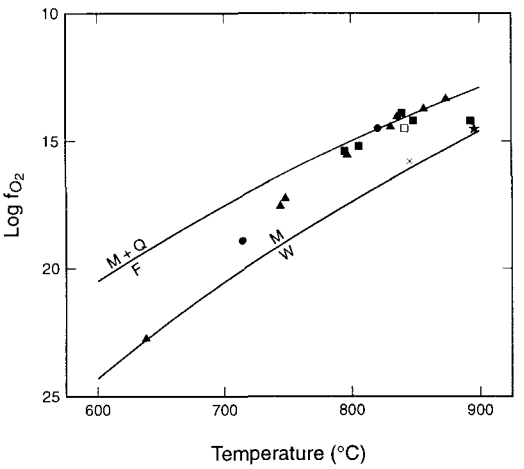

FIG. 12. Variation of log f_{O_2} and temperature based on the compositions of coexisting spinel and ilmenite. Also shown are curves for the fayalite-quartz-magnetite and magnetite-wustite buffers. Note the trend towards more reducing 'buffer' conditions in the main rock series as temperature falls, and the more reducing conditions shown by the oxides from the upper picrite and the granular olivine picrodolerite and associated pegmatite. Symbols as in Fig. 11.

essentially homogeneous *mg* values, Ni is zoned in olivine and Cr, Al and Ti show significant variations in pyroxene, while the plagioclase shows very extensive An-Ab zoning, particularly in the picrites. These differences clearly reflect the different diffusion rates for different elements in the minerals. The mg_{max} values for olivine in the picrites average about 83, with those in the picrodolerites being slightly lower (79). The olivine phenocrysts in the magma emplaced to form these parts of the sill are likely to have been somewhat more magnesian, but post-emplacement re-equilibration must have reset these values as Fe and Mg are known to diffuse comparatively quickly in olivine. However, Ni diffuses much more slowly in olivine and its zoning trend is likely to reflect incomplete re-equilibration. We have used high values for diffusion coefficients to obtain the minimum times to homogenize cation distributions. Smaller diffusion coefficients and different rate equations would give significantly longer timescales and a more detailed analysis will be considered in the companion paper (Gibb and Henderson, in prep.) in the context of a cooling model for the sill. However, although absolute diffusion rates would be different, the relative values for specific cations in specific minerals would be the same.

We have calculated minimum times for re-equilibrating 2 mm diameter olivine phenocrysts at 1200°C using the equation: $x = 4(Dt)$ (Kohn *et al.*, 1989), where x = diffusion distance (0.1 cm in this case), t = time, D = diffusion coefficient. Using the internally consistent diffusion coefficients calculated by Miyamota and Takeda (1981) for Mg, Fe and Ni of 3.0×10^{-12}, 48.0×10^{-12} and 0.8×10^{-12} cm^2s^{-1}, respectively, we estimate times for diffusive interchange between magma and the centre of the crystal of 3.1 yr for Mg, 0.4 yr for Fe, and 25 yr for Ni. The implication is that the picrite unit cooled to the blocking temperature for Mg-Fe inter-diffusion (close to the solidus temperature?) in something under 5 years which is slow enough to homogenize Fe and Mg but not Ni. During the *in-situ* cooling of the picrite, poikilitic pyroxenes and plagioclases coprecipitated. Pyroxene appears to have broadly similar Fe and Mg diffusion rates to those in olivine but Al and Ti diffusion in pyroxene should be much more sluggish as Si-Al exchange would be required, as is also the case in plagioclase. Based on measured diffusion coefficients for Al in diopside ($D = 3.7 \times 10^{-17}$ cm^2s^{-1} at 1180°C; Jaoul *et al.*, 1991) and the most rapid Al-Si disordering rates possible determined using deformation experiments ($D = 1.6 \times 10^{-18}$ cm^2s^{-1} at 1200°C; Kramer and Seifert, 1991), homogenization over a length scale of 100 μm would take about 5000 yr and 100,000 yr, respectively. Thus the zoning in these minerals shows that the cooling was too slow to prevent homogenization of Mg and Fe in pyroxene, but, not surprisingly, was too rapid to allow significant Al and Ti diffusion in pyroxene, and CaAl-NaSi diffusive exchange in plagioclase.

The upper picrites have kaersutite and evolved plagioclases which are slightly more K-rich than the equivalent phases in the lower picrites. We believe that such differences developed during late stage magmatic processes, after the picrite unit was divided by intrusion of the picrodolerite-crinanite unit, and resulted from late stage fluids from the evolved crinanites diffusing upwards into the upper picrite. The more Fe-rich olivines found in the upper picrite might have formed at this stage.

The lowermost picrodolerites show similar mineral compositional relations to those in the picrites, implying similar conditions of cooling and equilibration. However, within the crinanites the ophitic olivines have extremely strongly zoned Fe-Mg distributions, with a heterogeneity length scale of a few tens of microns in the outer parts of large ophitic crystals, implying that crystal growth rates far exceeded olivine component cation diffusion rates both within the crystal and melt (cf. for the growth of stongly zoned pyroxene crystals). Calculated times for diffusion of Mg and Fe on a length scale of 100 μm at 1200°C are 275 h for Mg and 36 h for Fe; equivalent diffusion times at 1100°C, perhaps a more realistic temperature, are 110 days for Mg and 15 days for Fe. If the diffusion data used are valid, the implication is that the sill cooled and crystallized very rapidly over the interval between emplacement temperature and solidus temperatures, even at the centre of the 140 m thick picrodolerite-crinanite unit, such that neither compositional nor textural equilibration were possible.

The conventional view of the cooling and differentiation of sills involves the inward movement of solidification fronts away from the cooling surfaces; phenocrysts might or might not escape from the upper 'capture front' depending on their gravitational settling velocities. Residual liquids generated within the leading edges of solidification fronts might be displaced inwards during this process. However, note that Marsh (this volume) has suggested "no phenocrysts, no post-emplacement differentiation". An interesting feature of the picrodolerite-crinanite unit is that, over a thickness of some 75 m (*70–145 m* levels), olivines, pyroxenes and plagioclases are all zoned over a similarly wide range of composition. It seems that to a large extent, the residual liquids are being retained; almost perfect fractional crystallization is occurring but on a local scale. Compositional convection and compaction are apparently not significant processes causing displacement of major amounts of residual liquids perpendicular to the solidification front. The only real

evidence for upward displacement of evolved liquids is found in existence of the main, although thin, pegmatite horizons within the topmost crinanites which are significantly less-differentiated than the crinanites below. These pegmatites are not in the correct place to be described as a 'sandwich horizon'. Marsh (this volume) has described similar occurrences of late-stage segregations from differentiated tholeiitic sills and suggested that they form within the upper solidification front by 'tearing apart' of earlier horizons, forming voids which are filled by upward movement of more evolved fluids from below. The Shiant Isles main pegmatites might have formed by similar mechanisms. The cross-cutting pegmatite veins associated with the picrites must have formed in a completely different way, probably by a proportion of the residual fluids escaping (by filter pressing?) into cooling fractures. Some of these veins cut the lower discontinuity showing that the late stage evolutionary history of the picrite overlapped with later-intruded picrodolerites being cool enough to have propagated cooling cracks.

The later stages of magmatic fractionation of the Shiant Isles rocks took place under distinctly reducing conditions as evidenced by the very reduced nature of the spinels in evolved crinanites and associated pegmatites (high ulvospinel and low magnetite), and by the pyroxene evolution being towards hedenbergite throughout rather than following a late trend towards aegirine enrichment. Indeed, Fe-rich pyroxenes are found in contact with analcime (originally nepheline?, see below) but Na_2O contents are normal and low (<1 wt.%), indicating very low contents of Fe^{3+} in the late stage melts. The only aegirine-rich pyroxenes occur in very small amounts as thin rims and tiny interstitial grains in a pegmatite which underwent significant deuteric alteration. The redox state of the picrodolerite-crinanite unit appears to have evolved to be even more reducing as evidenced by the proximity to the FMQ buffer during the early stages and MW during later stages. Most alkaline basaltic intrusions seem to follow cooling paths parallel to, and sometimes slightly on the more oxidized side, of the FMQ buffer (Nash and Wilkinson, 1970; Gamble, 1984; Henderson and Gibb, 1987). The Shiant Isles sill seems to become unusually reducing during the later stages.

Henderson and Gibb (1983) described the felsic mineral crystallization trends for a number of differentiated alkaline basaltic high-level intrusions. The Shiant Isles sill falls within the category of "Group I: Rocks containing a single, strongly zoned, Ca-Na-K feldspar". The magma stayed within the one feldspar field throughout its whole fractionation history and precipitated nepheline, either early or late depending on the bulk composition of the magma. Many of the intrusions contained a metastable, silica-rich nepheline which altered under subsolidus conditions to form the ubiquitous interstitial analcime. Wilkinson and Hensel (1994) subsequently described similar relationships for other alkali basaltic sills. We have not found any unaltered nepheline in Shiant Isles rocks, but do not doubt that it was once present and was the magmatic pre-cursor to the analcime. The deuteric alteration processes are more advanced in the Shiant Isles than in some other sills in that analcime is sometimes locally replaced by calcic zeolites (mainly thomsonite), and Ca-Na-K phillipsites also occur.

The formation of analcime and zeolites during the sub-solidus, hydrothermal stage was pervasive throughout the sill. Analcime veins are particularly abundant within the picrites and pegmatites, and zeolitic patches occur commonly at the top and bottom of the sill. Indeed, the outer margins tend to be more altered than rocks elsewhere in the sill, with the lower olivine teschenites and bottom-most picrite being pervasively hydrothermally altered. This extreme alteration is a common feature in high-level alkaline basaltic sills which we believe to be due to heated, convecting groundwaters being trapped below the sill and gaining access to the lower reaches of the sill following the formation of contraction joints during cooling (Gibb and Henderson, 1978; Dickin *et al.*, 1984; Henderson and Gibb, 1987). Fluids also gain access at the top of the sill as evidenced by such reactions as the replacement of Fe-Ti-oxides by sulphides (mainly pyrrhotite). Sulphide mineralization (pyrite, chalcopyrite or pentlandite) is also seen close to the bottom of the picrodolerites and in the pegmatites. It is possible that groundwaters gaining access to the sill following widespread jointing might have introduced sulphur from the country rocks. Such fluids might also have equilibrated with graphite in the sedimentary country rocks and contributed to the trends towards the more reduced magnetite-wustite buffer.

Acknowledgements

We thank Sally Gibson and Bruce Marsh for their constructive comments on this paper and Mike Cooper for drafting the figures by computer. David Plant and Tim Hopkins organized CMBH's microprobe work at Manchester. The field work and drilling were carried out during tenure of NERC research grant GR/3460.

References

Buddington, A.F. and Lindsley, D.H. (1964) Iron-titanium oxides and synthetic equivalents. *J. Petrol.*, **5**, 310–57.

Deer, W.A., Howie, R.A. and Zussman, J. (1978) *Rock-Forming Minerals: Vol 2a, Single-Chain Silicates.* Longman, London and New York, 668 pp.

Dickin, A.P., Henderson, C.M.B. and Gibb, F.G.F. (1984) Hydrothermal Sr contamination of the Dippin sill, Isle of Arran, Western Scotland. *Mineral. Mag.*, **48**, 311–22.

Drever, H.I. and Johnston, R. (1959) The lower margin of the Shiant Isles Sill. *Q. J. Geol. Soc. London,* **114**, 343–65.

Drever, H.I. and Johnston, R. (1965) New petrographical data on the Shiant Isles picrite. *Mineral. Mag.*, **34**, 194–203.

Gamble, J.A. (1984) Petrology and geochemistry of diiferentiated teschenite intrusions from the Hunter Valley, New South Wales, Australia. (1984) *Contrib. Mineral. Petrol.* **88**, 173–87.

Gibb, F.G.F. (1973) The zoned clinopyroxenes of the Shiant Isles Sill, Scotland. *J. Petrol.*, **14**, 203–30.

Gibb, F.G.F. and Gibson, S.A. (1989) The Little Minch sill complex. *Scott. J. Geol.*, **25**, 367–70.

Gibb, F.G.F. and Henderson, C.M.B. (1978) The petrology of the Dippin sill, Isle of Arran. *Scott. J. Geol.*, **14**, 1–27.

Gibb, F.G.F. and Henderson, C.M.B. (1984) The structure of the Shiant Isles sill complex, Outer Hebrides. *Scott. J. Geol.* **20**, 21–29.

Gibb, F.G.F. and Henderson, C.M.B. (1989) Discontinuities between picritic and crinanitic units in the Shiant Isles sill: evidence of multiple intrusion. *Geol. Mag.*, **126**, 127–37.

Gibb, F.G.F. and Henderson, C.M.B. (1992) Convection and crystal settling in sills. *Contrib. Min. Petrol.*, **109**, 538–45.

Gibson, S.A. and Jones, A.P. (1991) Igneous stratigraphy and internal structure of the Little Minch Sill Complex, Trotternish Peninsula, northern Skye, Scotland. *Geol. Mag.*, **128**, 51–66.

Helz, R.T. (1982) Experimental studies of amphibole stability. *Reviews in Mineralogy (Mineralogical Society of America, Washington),* **9B**, 279–353.

Henderson, C.M.B. and Gibb, F.G.F. (1983) Felsic mineral crystallization trends in differentiating alkaline basic magmas. *Contrib. Min. Petrol.*, **84**, 355–64.

Henderson, C.M.B. and Gibb, F.G.F. (1987) The petrology of the Lugar Sill, SW Scotland. *Trans. Roy. Soc. Edinbugh: Earth Sciences,* **77** (for 1986), 325–47.

Huppert, H.E. and Sparks, R.S.J. (1980) The fluid dynamics of a basaltic magma chamber replenished by influx of hot dense ultrabasic magma. *Contrib. Mineral. Petrol.*, **75**, 279–89.

Jaoul, O., Sautter, V. and Abel, F. (1991) Nuclear microanalysis: A powerful tool for measuring low atomic diffusivity with mineralogical applications. In: *Diffusion, atomic ordering, and mass transport* (J. Ganguly, ed.), *Advances in Physical Geochemistry,* **8**, 198–220, Springer, Dordrecht.

Johnston, R. (1953) The olivines of the Garbh Eilean sill, Shiant Isles. *Geol. Mag.*, **90**, 161–71.

Kitchen, D.E. (1985) The parental magma on Rhum — Evidence from alkaline segregations and veins in peridotites from Salisbury Dam. *Geol. Mag.*, **122**, 529–37.

Kohn, S.C., Henderson, C.M.B. and Mason, R.A. (1989) Element zoning trends in olivine phenocrysts from a supposed primary high-magnesian andesite: an electron- and ion-microprobe study. *Contrib. Mineral. Petrol.*, **103**, 242–52.

Kramer, M.J. and Seifert, K.E. (1991) Strain enhanced diffusion in feldspars. In: *Diffusion, atomic ordering, and mass transport* (J. Ganguly, ed.), *Advances in Physical Geochemistry,* **8**, 286–303, Springer, Dordrecht.

MacKenzie, W.S., Donaldson, C.H. and Guilford, C. (1982) *Atlas of Igneous Rocks and their Textures.* 148 pp. Longmans, Harlow, England.

Marsh, B.D. (1988) Crystal capture, sorting and retention in convecting magma. *Geol. Soc. Amer. Bull.*, **100**, 1720–37.

Marsh, B.D. (1989) On convective style and vigor in sheet-like magma chambers. *J. Petrol.*, **30**, 479–530.

Marsh, B. (1996) Solidification fronts and magmatic evolution. *Mineral. Mag.*, **60**, 5–40 (this volume).

Martin, D., Griffiths, R.W. and Campbell, I.H. (1987) Compositional and thermal convection in magma chambers. *Contrib. Mineral. Petrol.*, **96**, 465–75.

Miyamoto, M. and Takeda, H. (1983) Atomic diffusion coefficients calculated for transition metals in olivine. *Nature*, **303**, 602–3.

Murray, R.J. (1954) The clinopyroxenes of the Garbh Eilean sill, Shiant Isles. *Geol. Mag.*, **91**, 17–31.

Nash, W.P. and Wilkinson, J.F.G. (1970) Shonkin Sag laccolith, Montana, I. Mafic minerals and estimates of temperature, pressure, oxygen fugacity and silica activity. *Contrib. Mineral. Petrol.*, **25**, 241–69.

Powell, R. and Powell, M. (1977) Geothermometry and oxygen barometry using coexisting iron-titanium oxides: a reappraisal. *Mineral. Mag.*, **41**, 257–63.

Sparks, R.S.J., Huppert, H.E. and Turner, J.S. (1984) The fluid dynamics of evolving magma chambers. *Phil. Trans. R. Soc. London,* **A310**, 511–34.

Sparks, R.S., Huppert, H.E., Koyaguchi, T. and Hallworth, M.A. (1993) Origin of modal and rhythmic igneous layering by sedimentation in a convecting magma chamber. *Nature,* **361**, 246–9.

Tegner, C., Robins, B. and Sørensen, H.S. (1996) Crystallization from stratified magmas in the Honningsvåg Intrusive Suite, Northern Norway: a reappraisal. *Mineral. Mag.*, **60**, 41–51 (this volume).

Wager, L.R. and Brown, G.M. (1967) *Layered Igneous Rocks*, Oliver and Boyd, Edinburgh and London, 588 pp.

Walker, F. (1930) The geology of the Shiant Isles (Hebrides). *Q. J. Geol. Soc. London,* **86**, 355–98.

Wilkinson, J.F.G. (1956) Clinopyroxenes of alkali olivine basalt magma. *Amer. Mineral.*, **41**, 724–43.

Wilkinson, J.F.G. (1979) The mineralogy and petrography of alkali basaltic rocks. In: *The Alkaline Rocks* (H. Sørensen, ed.), Wiley Interscience, London, 67–95.

Wilkinson, J.F.G. and Hensel, H.D. (1994) Nephelines and analcimes in some igneous rocks. *Contrib. Mineral. Petrol.*, **118**, 79–91.

[*Revised manuscript received 10 July 1995*]